Two-dimensional spectroscopy. Application to nuclear magnetic resonance

W. P. Aue, E. Bartholdi, and R. R. Ernst

Laboratorium für physikalische Chemie, Eidgenössische Technische Hochschule, 8006 Zürich, Switzerland
(Received 13 November 1975)

The possibilities for the extension of spectroscopy to two dimensions are discussed. Applications to nuclear magnetic resonance are described. The basic theory of two-dimensional spectroscopy is developed. Numerous possible applications are mentioned and some of them treated in detail, including the elucidation of energy level diagrams, the observation of multiple quantum transitions, and the recording of high-resolution spectra in inhomogenous magnetic fields. Experimental results are presented for some simple spin systems.

I. INTRODUCTION

Spectroscopy in its classical form has been developed to investigate and to identify molecular systems in their linear approximation. Linearity is a crucial condition for the spectrum to uniquely represent the input/output relations of a physical system. It is particularly well fulfilled in optical spectroscopy as long as the use of lasers is disregarded. For linear systems, the entire apparatus of electronic system theory[1] can be employed to describe the methods of spectroscopy. Of particular importance is the equivalence of the notions "spectrum" and "transfer function" or "frequency response function," on one hand, and of "interferogram" or "free induction decay" and "impulse response," on the other. These correspondences proved to be fruitful in connection with the introduction of Fourier spectroscopy in optical spectroscopy[2] and in magnetic resonance.[3,4]

It is well known that linearity is merely an abstract concept to simplify the mathematical treatment. It does not correspond to physical reality, although it may be an excellent approximation, in many cases.

In radio frequency spectroscopy, linearity is restricted to very weak perturbations of the investigated system, and nonlinear effects are well known to occur in almost any spectroscopic radio frequency experiment. Typical effects are saturation effects, line broadening, and line shifts caused by strong perturbations.[5]

Some properties of molecular systems can only be noticed through nonlinear effects, e.g., spin–lattice relaxation and the connectivity of the various transitions in the energy level scheme. Spectroscopy has, therefore, been extended to include methods suitable for the investigation of nonlinear properties of molecular systems.

A straightforward extension of spectroscopy is the measurement of saturation curves and the analysis of line shapes under the influence of strong rf fields, although, in most cases, the information cannot be obtained directly but must be extracted by means of iterative approximation procedures.[6]

The most fruitful class of techniques was certainly provided by double resonance.[7,8] Here, a strong perturbation serves to modify the system in a nonlinear fashion. The actual spectroscopic experiment, using a second, weak perturbation, can again be considered as the investigation of a linear system. Of particular importance for the elucidation of the topology of energy level schemes and indirectly of molecular structure are techniques like spin tickling,[9] INDOR,[10] and selective population transfer.[11]

Another class of experiments aimed towards the investigation of nonlinear phenomena, particularly of relaxation mechanisms, is formed by pulse experiments which have been developed into a large variety of techniques of great practical importance.[3,12,13]

All these methods have been devised to measure specific properties connected with some nonlinear behavior of systems. In this paper, a very general class of techniques will be described which is suitable for a much wider characterization of nonlinear properties. Many of the earlier techniques are contained as special cases.

For the description of the nonlinear properties, it is not sufficient to consider just amplitude, perhaps including phase, as a function of frequency as it is done in classical spectroscopy. It is necessary to include at least one further parameter such as rf field strength, time, or a second frequency as is done, for example, in double resonance.[8] A graphic representation of such a set of data naturally leads to two-dimensional or, more generally, to multidimensional spectroscopy.

In the following, we will call a two-dimensional (or multidimensional) plot of spectral data a "two-dimensional (or multidimensional) spectrum" only when all variables of the plotted function are frequencies, in contrast, for example, to stacking, in a two-dimensional manner, a set of spectra as a function of time as is frequently done in relaxation time measurements.[13] Many possibilities to generate $2D$ spectra are conceivable. Some basic schemes are shown in Fig. 1.

(*a*) *Frequency space experiment.* The simultaneous application of two frequencies and measuring the response as a function of both frequencies leads directly to a $2D$ spectrum. This is the principle of conventional double resonance.[8] An example of a $2D$ tickling spectrum of the triplet of 1, 1, 2-trichloroethane is shown in Fig. 2. A complicated pattern of ridges of

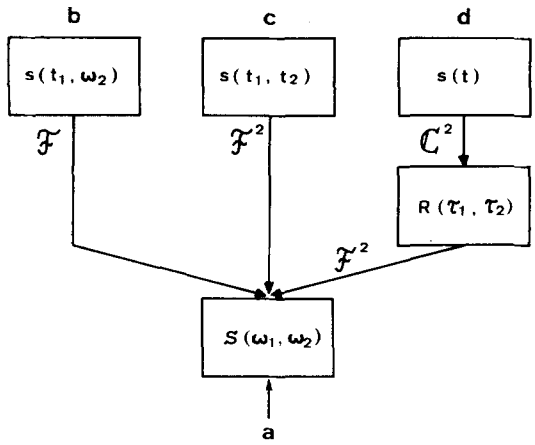

FIG. 1. Basic schemes to measure and compute 2D spectra. $\mathfrak{F}$ = Fourier transformation, $\mathfrak{C}$ = crosscorrelation.

changing amplitudes results. In addition, the pattern is strongly dependent on the rf field strength used.

(*b*) *Mixed frequency space time space experiment.* A system perturbed by a strong rf field with frequency ω_2 can be investigated by applying an rf pulse and measuring its response. Fourier transformation of the free induction decay and repetition of the experiment for various perturbing frequencies leads also to a 2*D* spectrum with properties very similar to those of conventional double resonance.[14,15]

(*c*) *Time space experiment.* A 2*D* experiment done completely in time space requires two independent time variables as a function of which a signal amplitude can be measured. A 2*D* Fourier transformation of the 2*D* time signal produces then again a 2*D* spectrum.[16,17]

(*d*) *Stochastic resonance experiment.* From the response of a nonlinear system to a Gaussian random perturbation, it is also possible to compute a 2*D* spectrum by calculating higher cross-correlation functions between input and output noise and Fourier transforming them.[18]

It is not intended to give a complete survey of all possibilities to create 2*D* spectra. This paper will be limited to the analysis of time space experiments which appear to be particularly fruitful. They are also of conceptual interest as they are generalizations of well-known pulse experiments and exhibit the essential features of these experiments in a particularly clear way.

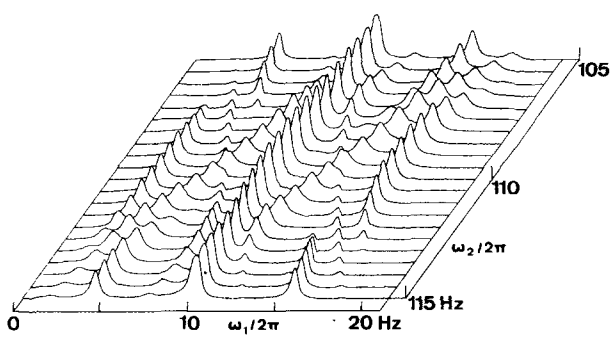

FIG. 2. Proton resonance 2*D* tickling spectrum of 1,1,2-trichloroethane. The doublet is irradiated at various frequencies ω_2; ω_1 is swept through the triplet part of the spectrum. A related 2*D* FTS spectrum is shown in Fig. 15.

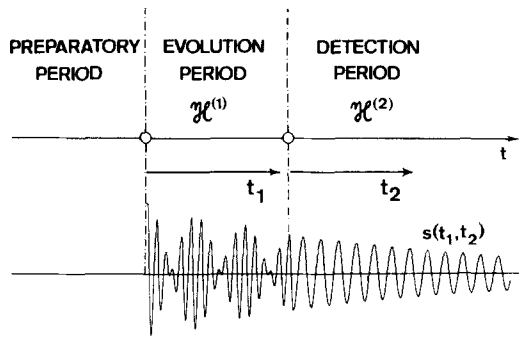

FIG. 3. Partitioning of the time axis in a 2*D* FTS experiment.

Section II gives a brief survey of some possibilities of 2*D* spectroscopy. The general theory of the basic experiment is described in Sec. III. Considerable simplifications are obtained by the restriction to weakly coupled systems. This is shown in Sec. IV. As an example of a strongly coupled spin system, the two-spin system is treated in Sec. V. Section VI is devoted to the phenomena in systems including equivalent spins, and Sec. VII describes the interesting features of 2*D* spectroscopy in the presence of inhomogeneous magnetic fields. Methods to observe zero quantum and double quantum transitions are treated in Sec. VIII. A few experimental aspects are mentioned in Sec. IX, although details on data processing in two dimensions and further applications will be described at another place.

It should be emphasized at this point that this work was stimulated by a presentation of Professor Jean Jeener at the Ampere International Summer School II, Basko Polje (1971), who mentioned the idea of the two-pulse version of 2*D* spectroscopy. The first experiments in Jeener's group were performed later by Alewaeters.[16]

II. TWO-DIMENSIONAL FOURIER SPECTROSCOPY

In 2*D* FTS, the 2*D* spectrum is obtained by Fourier transforming a signal $s(t_1, t_2)$ which depends on two independent time variables t_1 and t_2. For the introduction of two time variables, it is necessary to mark out two points on the time axis and to partition the experiment time into three periods. For the present purpose, it is convenient to let t_1 be the duration of the second period and t_2 the running time in the third period, as shown in Fig. 3. The signal $s(t_1, t_2)$ is then measured in the third period as a function of t_2 with t_1 as a parameter.

The three phases which are characteristic for all 2*D* FTS experiments are named according to their physical significance:

$t < 0$: *Preparation period.* The system is prepared in a suitable initial state, described by the density operator $\sigma(0)$.

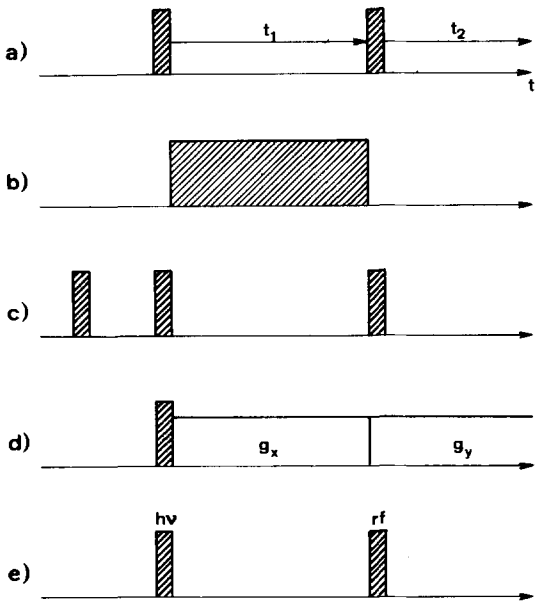

FIG. 4. Some homonuclear schemes for 2D FTS. (a) Basic two-pulse experiment. (b) Observation of Torrey oscillations. (c) Detection of a nonequilibrium state. (d) Fourier zeugmatography. (e) Detection of transient oscillations in CIDNP.

$0 < t < t_1$: *Evolution period.* The system evolves under the influence of the Hamiltonian $\mathcal{H}^{(1)}$ and assumes at the end of this interval a particular state which depends on $\mathcal{H}^{(1)}$ and on the elapsed time t_1.

$t_1 < t$: *Detection period.* The system develops further under the influence of the Hamiltonian $\mathcal{H}^{(2)}$. During this time, the transverse magnetization $M_y(t_1, t_2) = s(t_1, t_2)$ is detected as a function of t_2.

A large number of experiments for different duration t_1 of the evolution period have to be performed to obtain a sufficiently dense sampling of the 2D time function $s(t_1, t_2)$. In a multidimensional extension of 2D spectroscopy, the system has to go through several evolution periods, each of which must be varied systematically in its length.

Many homo- and heteronuclear experiments are possible which conform to this general scheme. Some possibilities are shown in Figs. 4 and 5. The basic experiment, suggested by Jeener,[16] is the two-pulse experiment of Fig. 4(a). The preparatory phase ends with a nonselective rf pulse at time $t = 0$ (called preparatory pulse). A flip angle of 90° is usually employed to generate off-diagonal elements of the density operator which evolve under the influence of the Hamiltonian $\mathcal{H}^{(1)}$ during the evolution period. This period is ended by a second rf field (called mixing pulse) at time $t = t_1$. It mixes the various magnetization components and enables their measurement during the detection period. This experiment permits elucidation of the energy level schemes of coupled spin systems. A very simple application is also the distinction of resonance lines belonging to different molecules in a mixture. A detailed analysis of this experiment is given in Sec. III.

In the experiment shown in Fig. 4(b), an rf field is applied during the evolution period. Separate preparation and mixing pulses are not required. During the evolution period, Torrey oscillations will develop. They can be associated with the various resonance transitions. A modification of this experiment, adding a magnetic field gradient during the detection period, may serve as a means to measure the spatial inhomogeneity of the rf field strength.

Figure 4(c) shows an experiment where a nonequilibrium state $\sigma(0)$ is created during the preparatory period. The first two pulses applied permit the population of all matrix elements of the density operator. The behavior during evolution and detection periods then completely characterizes the initial nonequilibrium state. Here, 2D spectroscopy is a means to measure the instantaneous state $\sigma(0)$ of a perturbed system, including the matrix elements responsible for the higher order transitions. An example of this experiment is analyzed in Sec. VIII.

Fourier zeugmatography may be considered as a special case of 2D (or 3D) spectroscopy.[19] Figure 4(d) shows a preparatory pulse which generates the required transverse magnetization which precesses during the following time periods in the presence of two different magnetic field gradients. It permits measurement of the 2D or 3D spatial spin density of macroscopic (biological) objects.

Nonequilibrium states can also be created by nonmagnetic perturbations, for example, by initiating a chemical reaction by means of a light pulse at time $t = 0$. Figure 4(e) indicates an experiment which has been

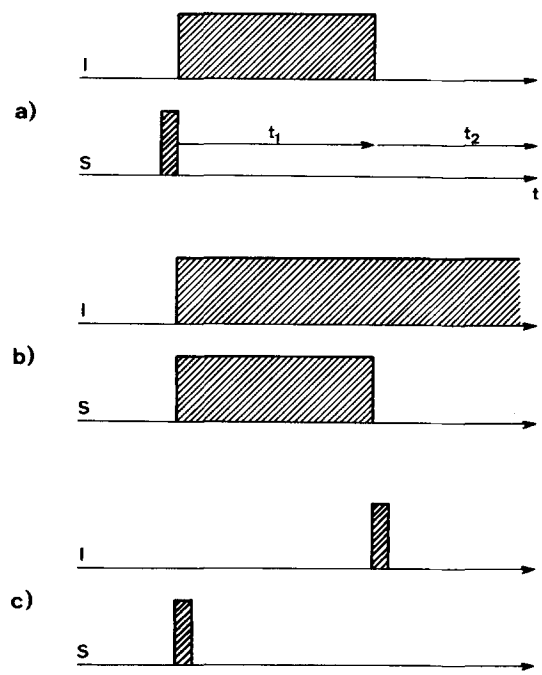

FIG. 5. Some heteronuclear schemes for 2D FTS. The S magnetization is observed. (a) 2D-resolved carbon-13 resonance. (b) Transitory cross polarization in solids. (c) Heteronuclear two-pulse experiment.

used to measure off-diagonal elements of the density operator $\sigma(0)$ created during the chemical reaction in chemically induced dynamic nuclear polarization.[20]

The heteronuclear experiment shown in Fig. 5(a) leads to 2*D*-resolved carbon-13 spectroscopy, a promising method to unravel complicated undecoupled carbon-13 spectra. During the evolution period, the ^{13}C spins precess in the absence of proton–carbon couplings while the complete Hamiltonian determines the evolution during the detection period. This permits separation of the multiplets which originate from different carbon spins.[21]

Figure 5(b) shows a typical cross-polarization experiment used in solids to detect rare nuclei.[22] The evolution period here is identical with the cross-polarization time. During this period, transient oscillations have recently been observed. They are caused by the coherent dipolar interaction of directly bound nuclei.[23] A 2*D* representation of these phenomena permits one to obtain structural information on solid samples, for single crystals as well as for powders. An interesting modification of this technique has recently been developed by Waugh.[24]

Figure 5(c), finally, sketches an experiment which is a heteronuclear modification of the basic two pulse experiment. It permits one to unravel the multiplet structure of heteronuclear spin systems. Many more modifications are conceivable involving pulsed and continuous rf fields, optical irradiations, magnetic field gradients or field jumps, and other perturbations leading to two- or multidimensional spectra.

In all these experiments, a 2*D* Fourier transformation is required to generate the desired complex 2*D* spectrum $S(\omega_1, \omega_2)$:

$$S(\omega_1, \omega_2) = \int_0^\infty dt_1 \exp(-i\omega_1 t_1) \int_0^\infty dt_2 [\exp(-i\omega_2 t_2)] s(t_1, t_2) \ . \tag{1}$$

It may be considered as a sum of four terms:

$$S(\omega_1, \omega_2) = S^{cc}(\omega_1, \omega_2) - S^{ss}(\omega_1, \omega_2) - iS^{cs}(\omega_1, \omega_2) - iS^{sc}(\omega_1, \omega_2) \ , \tag{2}$$

with, e.g.,

$$S^{cc}(\omega_1, \omega_2) = \int_0^\infty dt_1 \cos(\omega_1 t_1) \int_0^\infty dt_2 [\cos(\omega_2 t_2)] s(t_1, t_2) \ . \tag{3}$$

In many cases, it is more convenient to plot one of the four real components $S^{cc}(\omega_1, \omega_2)$, $S^{ss}(\omega_1, \omega_2)$, $S^{cs}(\omega_1, \omega_2)$, or $S^{sc}(\omega_1, \omega_2)$ instead of real or imaginary part of $S(\omega_1, \omega_2)$. $S^{cc}(\omega_1, \omega_2)$ can be considered as a four quadrant average of $S(\omega_1, \omega_2)$:

$$S^{cc}(\omega_1, \omega_2) = \tfrac{1}{4}\{S(\omega_1, \omega_2) + S(\omega_1, -\omega_2) + S(-\omega_1, \omega_2) + S(-\omega_1, -\omega_2)\} \ . \tag{4}$$

The following symmetry relations can easily be verified

$$S(-\omega_1, -\omega_2) = S(\omega_1, \omega_2)^* \ ,$$

$$S^{cc}(-\omega_1, \omega_2) = S^{cc}(\omega_1, -\omega_2) = S^{cc}(-\omega_1, -\omega_2) = S^{cc}(\omega_1, \omega_2) \ ,$$

$$-S^{ss}(-\omega_1, \omega_2) = -S^{ss}(\omega_1, -\omega_2) = S^{ss}(-\omega_1, -\omega_2) = S^{ss}(\omega_1, \omega_2) \ , \tag{5}$$

$$-S^{sc}(-\omega_1, \omega_2) = S^{sc}(\omega_1, -\omega_2) = -S^{sc}(-\omega_1, -\omega_2) = S^{sc}(\omega_1, \omega_2) \ ,$$

$$S^{cs}(-\omega_1, \omega_2) = -S^{cs}(\omega_1, -\omega_2) = -S^{cs}(-\omega_1, -\omega_2) = S^{cs}(\omega_1, \omega_2) \ .$$

In many applications, it is sufficient to compute the absolute value of $S(\omega_1, \omega_2)$ instead of plotting one of the phase sensitive components, e.g., $S^{cc}(\omega_1, \omega_2)$. The absolute value spectrum is much less critical to adjustment, but clearly, it contains less information. The absolute value spectrum $|S|(\omega_1, \omega_2)$ will be defined in the following particular manner:

$$|S|(\omega_1, \omega_2) = \tfrac{1}{2}[|S(\omega_1, \omega_2)|^2 + |S(\omega_1, -\omega_2)|^2 + |S(-\omega_1, \omega_2)|^2 + |S(-\omega_1, -\omega_2)|^2]^{1/2} \ . \tag{6}$$

This definition has the advantage that the contributions from all four quadrants will be taken into account, for, in some cases, peaks may contribute to two of the four quadrants only. Taking the absolute value spectrum, it is sufficient to plot one quadrant only. It can easily be shown that

$$|S|(\omega_1, \omega_2) = [S^{cc}(\omega_1, \omega_2)^2 + S^{cs}(\omega_1, \omega_2)^2 + S^{sc}(\omega_1, \omega_2)^2 + S^{ss}(\omega_1, \omega_2)^2]^{1/2} \ . \tag{7}$$

This equation is important for the numerical evaluation of experimental data.

III. THEORETICAL DESCRIPTION OF 2*D* FTS

In this section, a general 2*D* FTS experiment will be analyzed. At time $t = 0$, the system is assumed to be prepared in a state described by the density operator $\sigma(0)$. It can be an arbitrary nonequilibrium state.[20] During the time interval $0 < t < t_1$, the system develops freely under the influence of the time-independent Hamiltonian $\mathcal{H}^{(1)}$. At time $t = t_1$, the density operator is rotated by an rf pulse, represented by a superoperator[25] $\hat{\hat{R}}$. In special cases, this rf pulse may be absent [e.g., Figs. 4(b), 4(d), 5(a), and 5(b)]. During the remaining time, $t > t_1$, the system develops freely under the time-independent Hamiltonian $\mathcal{H}^{(2)}$. In many cases, $\mathcal{H}^{(1)} = \mathcal{H}^{(2)}$ [e.g., Figs. 4(a), 4(c), 4(e), and 5(c)]. In certain cases $\mathcal{H}^{(1)}$ and $\mathcal{H}^{(2)}$ can also represent time-independent Hamiltonians in a rotating frame [e.g., Figs. 4(b) and 5(b)].

The motion of the system is described by the density operator equation

$$\dot{\sigma} = -i[\mathcal{H}(t), \sigma] - \hat{\hat{\Gamma}}\{\sigma - \sigma_0(t)\} \ , \tag{8}$$

with

$$\mathcal{H}(t) = \begin{cases} \mathcal{H}^{(1)} \text{ for } 0 < t < t_1 \\ \mathcal{H}^{(2)} \text{ for } t > t_1, \end{cases} \text{ measured in frequency units.}$$

$\mathcal{H}^{(1)}$ and $\mathcal{H}^{(2)}$ are assumed to be high field Hamiltonians. The equilibrium density operator σ_0 may be different in the two time intervals,

$$\sigma_0(t) = \begin{cases} \sigma_0^{(1)} \text{ for } 0 < t < t_1 , \\ \sigma_0^{(2)} \text{ for } t > t_1 . \end{cases} \tag{9}$$

$\hat{\hat{\Gamma}}$ is the relaxation superoperator.

In a shorthand superoperator notation,[25] Eq. (8) can be written as

$$\dot{\sigma} = -\{i\hat{\hat{\mathcal{H}}}(t) + \hat{\hat{\Gamma}}\}\sigma + \hat{\hat{\Gamma}}\sigma_0(t) , \tag{10}$$

with

$$\hat{\hat{\mathcal{H}}}(t)\sigma = [\mathcal{H}(t), \sigma] .$$

This notation permits a straightforward solution for the density operator $\sigma(t_1, t_2)$ at time $t = t_1 + t_2$:

$$\sigma(t_1, t_2) = \sigma_0^{(2)} + \exp(-i\hat{\hat{\mathcal{H}}}^{(2)}t_2 - \hat{\hat{\Gamma}}t_2) \times [\hat{\hat{R}}\{\sigma_0^{(1)} + \exp(-i\hat{\hat{\mathcal{H}}}^{(1)}t_1 - \hat{\hat{\Gamma}}t_1)(\sigma(0) - \sigma_0^{(1)})\} - \sigma_0^{(2)}] . \tag{11}$$

The observed magnetization component, e.g., $M_y(t_1,t_2)$, is then given by

$$\begin{aligned} M_y(t_1, t_2) &= N\gamma\hbar \,\mathrm{Tr}[F_y\sigma(t_1, t_2)] \\ &= N\gamma\hbar \,\mathrm{Tr}[F_y \exp(-i\hat{\hat{\mathcal{H}}}^{(2)}t_2 - \hat{\hat{\Gamma}}t_2)\hat{\hat{R}}\{\sigma_0^{(1)} \\ &\quad + \exp(-i\hat{\hat{\mathcal{H}}}^{(1)}t_1 - \hat{\hat{\Gamma}}t_1)[\sigma(0) - \sigma_0^{(1)}]\}] . \end{aligned} \tag{12}$$

N is the number of spin systems per unit volume. The terms $\sigma_0^{(2)}$ and $\exp(-i\hat{\hat{\mathcal{H}}}^{(2)}t_2 - \hat{\hat{\Gamma}}t_2)\sigma_0^{(2)}$ usually do not contribute to the observed magnetization and have been neglected in Eq. (12). The $2D$ spectrum $S(\omega_1, \omega_2)$ is finally obtained by a $2D$ Fourier transformation of $M_y(t_1, t_2)$,

$$S(\omega_1, \omega_2) = \int_0^\infty dt_1\, e^{-i\omega_1 t_1} \int_0^\infty dt_2 e^{-i\omega_2 t_2} M_y(t_1, t_2) . \tag{13}$$

For the explicit evaluation, it proves to be convenient to separate $M_y(t_1, t_2)$ into the parts originating from the diagonal and off-diagonal parts of $\sigma(0)$, respectively. "Diagonal" and "off-diagonal" refer here to the Hamiltonian $\mathcal{H}^{(1)}$ which is assumed to possess nondegenerate eigenvalues. This separation can be effected by means of a pair of projection superoperators with the properties

$$\begin{aligned} &\hat{\hat{d}} + \hat{\hat{n}} = 1 , \\ &\hat{\hat{d}}^2 = \hat{\hat{d}}, \ \hat{\hat{n}}^2 = \hat{\hat{n}} , \\ &\hat{\hat{d}}\hat{\hat{\mathcal{H}}}^{(1)} = \hat{\hat{\mathcal{H}}}^{(1)} , \\ &[\hat{\hat{d}}A, \mathcal{H}^{(1)}] = 0 \text{ for any operator } A. \end{aligned} \tag{14}$$

One obtains

$$M_y(t_1, t_2) = M_y^d(t_1, t_2) + M_y^n(t_1, t_2) , \tag{15}$$

with

$$\begin{aligned} M_y^d(t_1, t_2) &= N\gamma\hbar \,\mathrm{Tr}[F_y \exp(-i\hat{\hat{\mathcal{H}}}^{(2)}t_2 - \hat{\hat{\Gamma}}t_2)\hat{\hat{R}}\{\sigma_0^{(1)} \\ &\quad + \exp(-i\hat{\hat{\mathcal{H}}}^{(1)}t_1 - \hat{\hat{\Gamma}}t_1)(\hat{\hat{d}}\sigma(0) - \sigma_0^{(1)})\}] , \end{aligned} \tag{16}$$

and

$$\begin{aligned} M_y^n(t_1, t_2) &= N\gamma\hbar \,\mathrm{Tr}[F_y \exp(-i\hat{\hat{\mathcal{H}}}^{(2)}t_2 - \hat{\hat{\Gamma}}t_2)\hat{\hat{R}} \\ &\quad \times \exp(-i\hat{\hat{\mathcal{H}}}^{(1)}t_1 - \hat{\hat{\Gamma}}t_1)\hat{\hat{n}}\sigma(0)] . \end{aligned} \tag{17}$$

$M_y^n(t_1, t_2)$ comprises those components which show an oscillatory behavior during the evolution period. They will, finally, be responsible for cross peaks and dia peaks in the $2D$ spectrum (see Fig. 6). These components contain the information which relates various transitions and which permits one to trace out the energy level diagram. $M_y^d(t_1, t_2)$, on the other hand, represents magnetization components which remain longitudinal during the evolution period and which do not oscillate during this time interval. $M_y^d(t_1, t_2)$ produces the axial peaks and provides information on spin–lattice relaxation processes.

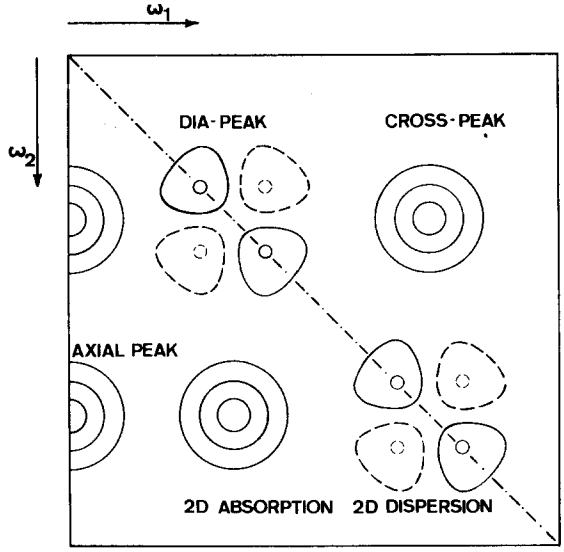

FIG. 6. Schematic representation of the features of a $2D$ spectrum.

A. Off-diagonal elements of $\sigma(0)$

In the absence of almost degenerate transitions and of partially overlapping lines, it is possible to neglect all parts of $\hat{\hat{\Gamma}}$ which do not commute with $\hat{\hat{\mathcal{H}}}$. It is, therefore, assumed that

$$[\hat{\hat{\mathcal{H}}}^{(1)}, \hat{\hat{\Gamma}}] = [\hat{\hat{\mathcal{H}}}^{(2)}, \hat{\hat{\Gamma}}] = 0 . \tag{18}$$

Taking into account that the relaxation superoperator $\hat{\hat{\Gamma}}$ (represented, e.g., by the Redfield relaxation matrix[26]) is a symmetric superoperator, i.e.,

$$\mathrm{Tr}\{A^\dagger\hat{\hat{\Gamma}}B\} = \mathrm{Tr}\{(\hat{\hat{\Gamma}}A)^\dagger B\} , \tag{19}$$

one obtains

$$\begin{aligned} M_y^n(t_1, t_2) &= N\gamma\hbar \,\mathrm{Tr}\{[\exp(i\hat{\hat{\mathcal{H}}}^{(2)}t_2 - \hat{\hat{\Gamma}}t_2)F_y] \\ &\quad \times \hat{\hat{R}}[\exp(-i\hat{\hat{\mathcal{H}}}^{(1)}t_1 - \hat{\hat{\Gamma}}t_1)\hat{\hat{n}}\sigma(0)]\} . \end{aligned} \tag{20}$$

In explicit notation, $M_y^n(t_1, t_2)$ is given by

$$\begin{aligned} M_y^n(t_1, t_2) &= N\gamma\hbar \sum_{kl}\sum_{mn} [F_{ykl} \exp(i\omega_{kl}^{(2)}t_2 - t_2/T_{2kl})] \\ &\quad \times R_{kl,mn}^{(21)}[(\hat{\hat{n}}\sigma(0))_{mn} \exp(-i\omega_{mn}^{(1)}t_1 - t_1/T_{2mn})] , \end{aligned} \tag{21}$$

with

$$\begin{aligned} &\omega_{mn}^{(1)} = \mathcal{H}_{mm}^{(1)} - \mathcal{H}_{nn}^{(1)} , \\ &\omega_{kl}^{(2)} = \mathcal{H}_{kk}^{(2)} - \mathcal{H}_{ll}^{(2)} . \end{aligned}$$

In the absence of overlapping lines, each transition possesses a single relaxation time T_{2kl}. The matrix elements of F_y are computed in the eigenbase of $\mathcal{H}^{(2)}$, whereas the matrix elements of $(\hat{\hat{n}}\sigma(0))$ are evaluated in the eigenbase of $\mathcal{H}^{(1)}$. The matrix elements of the superoperator $\hat{\hat{R}}$ are, therefore, calculated in a mixed base. This is indicated by the index (21) on $R^{(21)}_{kl,mn}$. It is assumed that $\hat{\hat{R}}$ causes a rotation by the angle α around the x axis. It is then possible to give an explicit expression for $R^{(21)}_{kl,mn}$:

$$R^{(21)}_{kl,mn} = \sum_p \sum_q R_{pm} R^*_{qn} T_{qk} T^*_{pl} \ . \tag{22}$$

R_{pm} and R_{qn} are matrix elements of the rotation operator

$$R = \exp(-i\alpha F_x) \ , \tag{23}$$

taken in the eigenbase of $\mathcal{H}^{(1)}$, and T_{qk} and T_{pl} are matrix elements of the transformation operator relating the eigenbases $\{e^{(1)}_k\}$ and $\{e^{(2)}_k\}$ of the Hamiltonians $\mathcal{H}^{(1)}$ and $\mathcal{H}^{(2)}$, respectively:

$$(e^{(2)}_1, e^{(2)}_2, \ldots) = (e^{(1)}_1, e^{(1)}_2, \ldots) \cdot T \ . \tag{24}$$

Equation (21) clearly shows the structure of $M^n_y(t_1,t_2)$. It consists of a sum of bilinear terms in damped oscillations originating from the Hamiltonians $\mathcal{H}^{(1)}$ and $\mathcal{H}^{(2)}$. The amplitudes of oscillation are determined by the matrix elements of $\sigma(0)$ and F_y, respectively. The bilinear coupling coefficients are provided by the superoperator $\hat{\hat{R}}$. The oscillation frequencies $\omega^{(1)}_{mn}$, can in general, comprise all possible transition frequencies of $\mathcal{H}^{(1)}$, including the forbidden zero-, double-, and multiple-quantum transitions. The oscillation frequencies $\omega^{(2)}_{kl}$, on the other hand, are limited to the allowed single quantum transitions of $\mathcal{H}^{(2)}$.

Of primary interest are the contributions to specific peaks in the 2D spectrum. $M^n_y(t_1, t_2)$ will therefore be split into a sum of contributions $M^n_{y\,kl,mn}(t_1, t_2)$ which relate the transitions $\omega^{(2)}_{kl}$ and $\omega^{(1)}_{mn}$:

$$M^n_y(t_1, t_2) = \sum_{kl} \sum_{mn} M^n_{y\,kl,mn}(t_1, t_2) \ , \tag{25}$$

and

$$M^n_{y\,kl,mn}(t_1, t_2) = Z_{kl,mn} \exp(i\omega^{(2)}_{kl} t_2 - t_2/T_{2kl}) \times \exp(-i\omega^{(1)}_{mn} t_1 - t_1/T_{2mn}) \ . \tag{26}$$

$Z_{kl,mn}$ are the complex signal amplitudes with

$$Z_{kl,mn} = N\gamma\hbar F_{ykl} R^{(21)}_{kl,mn} (\hat{\hat{n}}\sigma(0))_{mn} \ . \tag{27}$$

They are the central quantities which have to be computed later on.

The contributions to one specific peak in the 2D spectrum $S(\omega_1, \omega_2)$ are obtained by Fourier-transforming $M^n_{y\,kl,mn}(t_1, t_2)$:

$$\begin{aligned} S_{kl,mn}(\omega_1, \omega_2) &= \int_0^\infty dt_1 \, e^{-i\omega_1 t_1} \int_0^\infty dt_2 e^{-i\omega_2 t_2} M^n_{y\,kl,mn}(t_1, t_2) \\ &= Z_{kl,mn} [a^{(2)}_{kl}(\omega_2) - i d^{(2)}_{kl}(\omega_2)] \\ &\quad \times [a^{(1)}_{nm}(\omega_1) - i d^{(1)}_{nm}(\omega_1)] \ , \end{aligned} \tag{28}$$

with

$$a^{(2)}_{kl}(\omega_2) = \frac{1/T_{2kl}}{(\omega_2 - \omega^{(2)}_{kl})^2 + 1/T^2_{2kl}} \ ;$$

$$d^{(2)}_{kl}(\omega_2) = (\omega_2 - \omega^{(2)}_{kl}) / [(\omega_2 - \omega^{(2)}_{kl})^2 + 1/T^2_{2kl}] \ .$$

Equation (28) shows that neither real nor imaginary parts of the complex spectrum will ever be of pure 2D absorptive or dispersive character but that a more complicated line shape will be obtained. For the real part, one obtains, for example:

$$\begin{aligned} \mathrm{Re}\{S_{kl,mn}(\omega_1, \omega_2)\} &= \mathrm{Re}\{Z_{kl,mn}\} [a^{(2)}_{kl}(\omega_2) a^{(1)}_{nm}(\omega_1) \\ &\quad - d^{(2)}_{kl}(\omega_2) d^{(1)}_{nm}(\omega_1)] \\ &\quad + \mathrm{Im}\{Z_{kl,mn}\} [d^{(2)}_{kl}(\omega_2) a^{(1)}_{nm}(\omega_1) \\ &\quad + a^{(2)}_{kl}(\omega_2) d^{(1)}_{nm}(\omega_1)] \ . \end{aligned} \tag{29}$$

To avoid these complicated mixed line shapes, it is of advantage to utilize a real 2D cosine Fourier transformation and to plot $S^{cc}(\omega_1, \omega_2)$ [Eq. (3)]. According to Eq. (5), $S^{cc}(\omega_1, \omega_2)$ is even in two dimensions. The information in all four quadrants is identical.

The four peaks generated by each pair of transitions (kl) and (mn), one in each quadrant, are conveniently combined in one single term $S^{cc}_{(kl)(mn)}(\omega_1, \omega_2)$:

$$\begin{aligned} S^{cc}_{(kl)(mn)}(\omega_1, \omega_2) &= S^{cc}_{kl,mn}(\omega_1, \omega_2) + S^{cc}_{kl,nm}(\omega_1, \omega_2) \\ &\quad + S^{cc}_{lk,mn}(\omega_1, \omega_2) + S^{cc}_{lk,nm}(\omega_1, \omega_2) \ . \end{aligned} \tag{30}$$

The terms $S^{cc}_{kl,mn}(\omega_1, \omega_2)$ are related to $S_{kl,mn}(\omega_1, \omega_2)$ through Eq. (4). The signal contribution $S^{cc}_{(kl)(mn)}(\omega_1, \omega_2)$ can be written in the form

$$\begin{aligned} S^{cc}_{(kl)(mn)}(\omega_1, \omega_2) &= A_{(kl)(mn)} \{a^{(2)}_{kl}(\omega_2) + a^{(2)}_{lk}(\omega_2)\} \{a^{(1)}_{mn}(\omega_1) + a^{(1)}_{nm}(\omega_1)\} + B_{(kl)(mn)} \{-d^{(2)}_{kl}(\omega_2) + d^{(2)}_{lk}(\omega_2)\} \{-d^{(1)}_{mn}(\omega_1) + d^{(1)}_{nm}(\omega_1)\} \\ &\quad + C_{(kl)(mn)} \{a^{(2)}_{kl}(\omega_2) + a^{(2)}_{lk}(\omega_2)\} \{-d^{(1)}_{mn}(\omega_1) + d^{(1)}_{nm}(\omega_1)\} + D_{(kl)(mn)} \{d^{(2)}_{kl}(\omega_2) - d^{(2)}_{lk}(\omega_2)\} \{a^{(1)}_{mn}(\omega_1) + a^{(1)}_{nm}(\omega_1)\} \ . \end{aligned} \tag{31}$$

Here, (kl) and (mn) are ordered pairs of indices with $M_k \geq M_l$ and $M_m \geq M_n$. M_k is the magnetic quantum number of state k. This notation reduces the number of terms in the summation for the signal $S^{cc}(\omega_1, \omega_2)$ by a factor of 4. Similar expressions can be obtained for the 2D sine and mixed sine–cosine transforms, $S^{ss}_{(kl)(mn)}(\omega_1, \omega_2)$, $S^{cs}_{(kl)(mn)}(\omega_1, \omega_2)$, and $S^{sc}_{(kl)(mn)}(\omega_1, \omega_2)$.

The real amplitudes $A_{(kl)(mn)}, \ldots, D_{(kl)(mn)}$ of Eq. (31) are related to the complex amplitudes $Z_{kl,mn}$, defined in Eq. (27), by

$$\begin{aligned} A_{(kl)(mn)} &= \tfrac{1}{2} \mathrm{Re}\{Z_{kl,mn} + Z_{lk,mn}\} \ , \\ B_{(kl)(mn)} &= \tfrac{1}{2} \mathrm{Re}\{Z_{kl,mn} - Z_{lk,mn}\} \ , \\ C_{(kl)(mn)} &= \tfrac{1}{2} \mathrm{Im}\{Z_{kl,mn} + Z_{lk,mn}\} \ , \\ D_{(kl)(mn)} &= \tfrac{1}{2} \mathrm{Im}\{Z_{kl,mn} - Z_{lk,mn}\} \ , \end{aligned} \tag{32}$$

utilizing the property $Z_{kl,mn} = Z^*_{lk,nm}$. The virtue of Eq. (31) is that, for proper phase adjustment, only one term remains, so that peaks with a pure phase can be obtained. For phase adjustment, it is necessary to form linear combinations of $S^{cc}_{(kl)(mn)}$, $S^{ss}_{(kl)(mn)}$, $S^{cs}_{(kl)(mn)}$, and $S^{sc}_{(kl)(mn)}$.

The absolute signal amplitudes [compare Eq. (6)], given by

$$|Z|_{kl,mn} = \tfrac{1}{2}[|Z_{kl,mn}|^2 + |Z_{kl,nm}|^2 + |Z_{lk,mn}|^2 + |Z_{lk,nm}|^2]^{1/2}, \tag{33}$$

can also be expressed by the real amplitudes $A_{(kl)(mn)}$, $\ldots, D_{(kl)(mn)}$:

$$|Z|_{kl,mn} = [A^2_{(kl)(mn)} + B^2_{(kl)(mn)} + C^2_{(kl)(mn)} + D^2_{(kl)(mn)}]^{1/2} . \tag{34}$$

Two different kinds of peaks can be distinguished which originate from $S_{kl,mn}(\omega_1, \omega_2)$ (see Fig. 6):

(i) *Cross peaks*: they occur for $(kl) \neq (mn)$ and correlate different transitions. These are the "off-diagonal" peaks in a 2*D* spectrum; and

(ii) *Dia peaks*: they occur for $(kl) = (mn)$ and are related to one single transition, only. They occur on the main diagonal of the 2*D* spectrum.

Cross and dia peaks contain three kinds of information:

(a) *Information about the connectivity of transitions in the energy level diagram.* This information is analogous to the one obtained from double resonance, particularly from tickling experiments.[9] It is provided by the rotation superoperator $\hat{\hat{R}}$ which couples the various transitions. Particularly informative is also the flip angle dependence of intensities and phases. 2*D* spectra contain a wealth of information on the topology of the energy level diagram;

(b) *Information on transverse relaxation processes.* The line shapes are determined by the transverse relaxation times T_{2kl}. As will be shown later, they can also be determined even in the presence of field inhomogeneity broadening;

(c) *Information on the initial state* $\sigma(0)$ *of the spin system.* In conventional spectroscopy, allowed transitions can be detected only. In 2*D* FTS, on the other hand, it is possible to measure all matrix elements of $\sigma(0)$ in a unique manner. Particularly, it is possible to observe matrix elements responsible for zero-, double- and multiple-quanta transitions. This will be shown in Sec. VIII.

B. Diagonal elements of $\sigma(0)$

The contributions of the $M^d_y(t_1, t_2)$ term, which leads to the axial peaks, will now be evaluated in a similar manner. With Eq. (18), one obtains from Eq. (16)

$$M^d_y(t_1, t_2) = N\gamma\hbar \,\mathrm{Tr}\{[\exp(i\hat{\hat{\mathcal{H}}}^{(2)} t_2 - \hat{\hat{\Gamma}} t_2) F_y] \hat{\hat{R}} [\sigma_0^{(1)} + \exp(-\hat{\hat{\Gamma}} t_1) \cdot (\hat{\hat{d}}\sigma(0) - \sigma_0^{(1)})]\} , \tag{35}$$

and in explicit matrix notation

$$M^d_y(t_1, t_2) = N\gamma\hbar \sum_{kl} \sum_m [F_{ykl} \exp(i\omega^{(2)}_{kl} t_2 - t_2/T_{2kl})] R^{(21)}_{kl,mm} \times [P_{om} + \sum_n (\exp(-Wt_1))_{mn} \{P_n(0) - P_{on}\}] . \tag{36}$$

Here, the diagonal elements of the density operator in the eigenbase of $\mathcal{H}^{(1)}$ have been identified with the population numbers P_n:

$$P_n(0) = \sigma_{nn}(0), \; P_{on} = \sigma^{(1)}_{onn}, \tag{37}$$

and W is the Redfield relaxation matrix[26] which describes the longitudinal relaxation in a coupled nuclear spin system with

$$W_{ik} = \Gamma_{iikk} . \tag{38}$$

The matrix elements of $\exp(-Wt_1)$ can be expressed by the eigenvalues w_j of W:

$$[\exp(-Wt_1)]_{mn} = \sum_j S_{mj} S^*_{nj} \exp(-w_j t_1) , \tag{39}$$

with S representing the diagonalizing transformation of W.

$M^d_y(t_1, t_2)$ will now be split into the various contributions to particular resonance peaks:

$$M^d_y(t_1, t_2) = \sum_{kl} M^d_{ykl}(t_1, t_2) + \sum_{kl} \sum_j M^d_{ykl,j}(t_1, t_2) , \tag{40}$$

with

$$M^d_{ykl}(t_1, t_2) = G_{kl} \exp(i\omega^{(2)}_{kl} t_2 - t_2/T_{2kl}) , \tag{41}$$

and

$$M^d_{ykl,j}(t_1, t_2) = G_{kl,j} \exp(i\omega^{(2)}_{kl} t_2 - t_2/T_{2kl}) \exp(-w_j t_1) . \tag{42}$$

The coefficients are given by

$$G_{kl} = N\gamma\hbar F_{ykl} \sum_m R^{(21)}_{kl,mm} P_{om}$$
$$G_{kl,j} = N\gamma\hbar F_{ykl} \sum_m \sum_n R^{(21)}_{kl,mm} S_{mj} S^*_{nj} (P_n(0) - P_{on}) . \tag{43}$$

Equation (41) shows that $M^d_{ykl}(t_1, t_2)$ is independent of t_1. To obtain a nondiverging Fourier integral, it is therefore necessary to limit the integration to $0 < t_1 < t_m$ where t_m is a suitable upper limit for t_1. Then, one obtains

$$S_{kl}(\omega_1, \omega_2) = G_{kl}\{a^{(2)}_{kl}(\omega_2) - i d^{(2)}_{kl}(\omega_2)\} \frac{1}{\omega_1} \{\sin\omega_1 t_m - i(1 - \cos\omega_1 t_m)\} .$$
$$S_{kl,j}(\omega_1, \omega_2) = G_{kl,j}\{a^{(2)}_{kl}(\omega_2) - i d^{(2)}_{kl}(\omega_2)\}\{w_j/(\omega_1^2 + w_j^2) - i\omega_1/(\omega_1^2 + w_j^2)\} . \tag{44}$$

Of particular interest is again the 2*D* cosine transform of $M^d_y(t_1, t_2)$. Here, one obtains the following contributions

$$S^{cc}_{(kl)}(\omega_1, \omega_2) = [\mathrm{Re}\{G_{kl}\}\{a^{(2)}_{kl}(\omega_2) + a^{(2)}_{lk}(\omega_2)\} - \mathrm{Im}\{G_{kl}\}\{-d^{(2)}_{kl}(\omega_2) + d^{(2)}_{lk}(\omega_2)\}] \times \frac{1}{\omega_1} \sin\omega_1 t_m , \tag{45}$$

$$S^{cc}_{(kl),j}(\omega_1,\omega_2)=[\mathrm{Re}\{G_{kl,j}\}\{a^{(2)}_{kl}(\omega_2)+a^{(2)}_{lk}(\omega_2)\} - \mathrm{Im}\{G_{kl,j}\}\{-d^{(2)}_{kl}(\omega_2)+d^{(2)}_{lk}(\omega_2)\}] \times \frac{w_j}{\omega_1^2+w_j^2} \quad . \tag{46}$$

Equations (45) and (46) describe contributions to the $2D$ spectrum which all lie on the ω_2 axis ($\omega_1=0$). These peaks are called axial peaks (see Fig. 6). Each allowed transition $\omega^{(2)}_{kl}$ is represented by a peak which itself is a superposition of Lorentzians with half-width w_j in the ω_1 direction and which also contains a contribution proportional to $(1/\omega_1)\sin\omega_1 t_m$. The line shape, therefore, contains "T_1" information although, particularly in complicated spin systems, it may be difficult to be extracted.

The complete $2D$ spectrum is finally obtained as a sum of the contributions from Eqs. (31), (45), and (46):

$$S^{cc}(\omega_1,\omega_2)=\sum_{(kl)}\sum_{(mn)}S^{cc}_{(kl)(mn)}(\omega_1,\omega_2)+\sum_{(kl)}S^{cc}_{(kl)}(\omega_1,\omega_2) + \sum_{(kl)}\sum_{j}S^{cc}_{(kl),j}(\omega_1,\omega_2) \quad . \tag{47}$$

The first term describes the cross and dia peaks, whereas second and third terms contribute to the axial peaks.

IV. WEAKLY COUPLED HOMONUCLEAR SYSTEMS

For weak coupling among N nonequivalent spins $\frac{1}{2}$, it is possible to derive closed expressions for intensities and phases in a $2D$ spectrum. This case provides an instructive insight into the features of $2D$ spectroscopy. To simplify the situation, it is assumed that the initial state $\sigma(0)$ is prepared by means of a 90°_x pulse acting on a system in thermodynamic equilibrium. This produces the initial state

$$\sigma(0)=\frac{1+(\hbar\omega_0/kT)F_y}{\mathrm{Tr}\{1\}} \quad . \tag{48}$$

Additionally, $\mathcal{H}^{(2)}$ is set equal to $\mathcal{H}^{(1)}$. Then, one obtains for the complex signal amplitude $Z_{kl,mn}$ with Eqs. (22), (23), and (27)

$$Z_{kl,mn}=Q\cdot F_{ykl}R_{lm}R^*_{kn}F_{ymn} \text{ with } Q=\frac{N\gamma\hbar^2\omega_0}{kT\,\mathrm{Tr}\{1\}} \quad . \tag{49}$$

For spin $\frac{1}{2}$, the matrix elements F_{ykl} are given by

$$F_{ykl}=\begin{cases}\frac{1}{2}i(M_l-M_k) & \text{for allowed transitions with a single spin flipping, } \Delta m_s=\pm1 \text{ and } \Delta m_r=0 \text{ for } r\neq s\\ 0 & \text{for all forbidden transitions.}\end{cases}$$

Here, M_l is the magnetic quantum number of state l, and the matrix elements of the rotation operator R are found to be[20]

$$R_{lm}=(-i\sin\tfrac{1}{2}\alpha)^{\Delta_{lm}}(\cos\tfrac{1}{2}\alpha)^{N-\Delta_{lm}} \quad , \tag{50}$$

where Δ_{lm}, the spin flip number, is the number of spins with different spin polarization in the two states l and m. With Eqs. (49) and (50), one obtains for $Z_{kl,mn}$

$$Z_{kl,mn}=-\tfrac{1}{4}Q\cdot(-1)^{\Delta_{lm}}(i)^{\Delta_{lm}+\Delta_{kn}}[\sin\tfrac{1}{2}\alpha]^{\Delta_{lm}+\Delta_{kn}} \times[\cos\tfrac{1}{2}\alpha]^{2N-\Delta_{lm}-\Delta_{kn}}(M_l-M_k)(M_n-M_m) \quad , \tag{51}$$

for pairs of allowed transitions (kl) and (mn). By means of Eq. (32), it is finally possible to compute the real amplitudes $A_{(kl)(mn)},\ldots,D_{(kl)(mn)}$. It is seen from Eq. (51) that $Z_{kl,mn}$ is either real or imaginary. Therefore, two of the real amplitudes are necessarily zero. For transitions with $\Delta M=\pm1$, $Z_{kl,mn}$ is found to be real and $C_{(kl)(mn)}=D_{(kl)(mn)}=0$.

For the amplitudes G_{kl} and $G_{kl,j}$ of the longitudinal contributions, one obtains similarly

$$G_{kl}=-\frac{i}{2}Q\cdot\sum_m(-1)^{\Delta_{lm}}(i)^{\Delta_{lm}+\Delta_{km}}[\sin\tfrac{1}{2}\alpha]^{\Delta_{lm}+\Delta_{km}} \times[\cos\tfrac{1}{2}\alpha]^{2N-\Delta_{lm}-\Delta_{km}}M_m(M_l-M_k) \quad , \tag{52}$$

and

$$G_{kl,j}=\frac{i}{2}Q\cdot\sum_m\sum_n(-1)^{\Delta_{lm}}(i)^{\Delta_{lm}+\Delta_{km}}[\sin\tfrac{1}{2}\alpha]^{\Delta_{lm}+\Delta_{km}} \times[\cos\tfrac{1}{2}\alpha]^{2N-\Delta_{lm}-\Delta_{kn}}S_{mj}S^*_{nj}M_n(M_l-M_k) \quad . \tag{53}$$

To obtain a better understanding of the complex amplitudes $Z_{kl,mn}$ [Eq. (51)] it is convenient to introduce connectivity classes to distinguish various pairs of transitions.

For a general description of connectivity in weakly coupled spin systems, it is necessary to indicate all spin states for the two transitions in question. The following notation is used here: (1) the two transitions in question are indicated by the letter of the flipping spin. To identify the particular transition, the lower magnetic quantum number of the two connected states is indicated by a subscript. For nonequivalent spins $\frac{1}{2}$, no indexing is required; (2) within brackets, the states of all other spins are indicated by their magnetic quantum numbers. For nonequivalent spins $\frac{1}{2}$, + and − are used to fix the spin state; and (3) for magnetically equivalent nuclei, the group spin quantum number (irreducible representation of the permutation group) is indicated additionally by a superscript.

Some examples are:

(1) 4 nonequivalent spins $\frac{1}{2}$:

$[A(B_+C_+D_-),B(A_-C_-D_+)]$;

(2) A_2X_3 system:

$[A^{(1)}_{-1}(X^{(3/2)}_{1/2}),X^{(3/2)}_{-3/2}(A^{(1)}_0)]$.

For weakly coupled, nonequivalent spins $\frac{1}{2}$, it is possible to distinguish three classes of connectivity patterns. Their definition follows the well-known terminology used for directly connected transitions, distinguishing regressive and progressive transitions.[8] These notions are generalized in the following manner (see Fig. 7):

(*a*) *Parallel pairs*: The *same* spin flips in both transitions:

e.g., $[A(B_+C_+D_-),A(B_-C_+D_+)]$;

(*b*) *Regressive pairs*: two *different* spins A and B flip in the two transitions. A and B appear with the

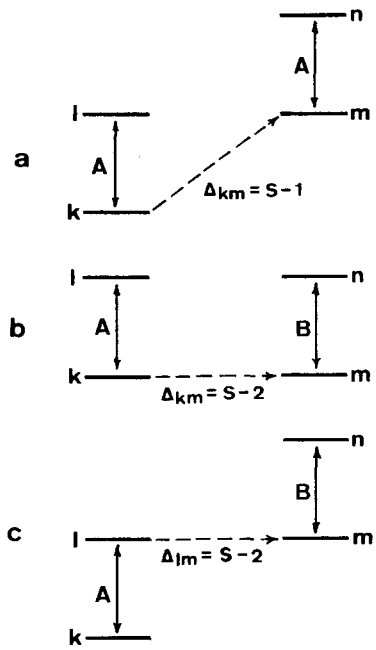

FIG. 7. Definitions of connectivity classes for nonequivalent spins $\frac{1}{2}$. (a) Parallel pair, two A spin transitions; along the broken line S-1 spins ($\neq A$) change their polarization. (b) Regressive pair, one A and one B spin transition; along the broken line S-2 spins ($\neq A, B$) change their polarization. (c) Progressive pair, one A and one B spin transition; along the broken line, S-2 spins ($\neq A, B$) change their polarization.

same polarization in the inner brackets:

e.g., $[A(B_+C_+D_-), B(A_+C_-D_+)]$;

(c) *Progressive pairs*: two *different* spins A and B flip in the two transitions, A and B appear with *different* polarization in the inner brackets:

e.g., $[A(B_+C_+D_-), B(A_-C_-D_+)]$.

Regressive and progressive connectivity reduce to the former notion when the transitions are directly connected. For indirectly connected transitions, regressive and progressive pairs are defined such that the elimination of all spins which do not flip in either transition reduces the pair to a directly connected regressive or progressive pair, respectively.

A convenient shorthand notation considers only (1) the number of spins S necessary to describe a certain connection (disregarding spins which neither flip nor have different polarization in the two transitions); (2) the connectivity character (l = parallel, r = regressive, p = progressive); and (3) the total number of coupled spins. Examples are:

$[A(B_+C_+D_-), A(B_-C_+D_+)] \rightarrow 3l4$,

$[A(B_+C_+D_-), B(A_+C_-D_+)] \rightarrow 4r4$,

$[A(B_+C_+D_-), B(A_-C_-D_-)] \rightarrow 3p4$.

This is the entire information which is necessary to compute peak intensities in a 2D spectrum, or, in other words, it is all the information which can be obtained from a 2D spectrum.

The spin flip numbers Δ_{lm} used in Eq. (50) depend only on S and on the connectivity character, and are given by the following values:

Connection	Δ_{lm}	Δ_{kn}	Δ_{km}	Δ_{ln}
parallel	S	S	$S-1$	$S-1$
regressive	$S-1$	$S-1$	S or $S-2$	$S-2$ or S
progressive	S or $S-2$	$S-2$ or S	$S-1$	$S-1$

These values can easily be checked by inspection of Fig. 7. A distinction of the two cases indicated for both regressive and progressive pairs is immaterial since the same signal amplitudes will result in both cases.

This leads, finally, to the following simple relations for the complex signal amplitudes $Z_{kl,mn}$, and for the real amplitudes $A_{(kl)(mn)}$ and $B_{(kl)(mn)}$ used in Eq. (31) ($C_{(kl)(mn)} = D_{(kl)(mn)} = 0$ for single quantum transitions):

(a) *Parallel pairs* (SlN):

$$Z_{kl,mn} = -\tfrac{1}{4}Q(\sin\tfrac{1}{2}\alpha)^{2S}(\cos\tfrac{1}{2}\alpha)^{2N-2S} ,$$
$$Z_{lk,mn} = \tfrac{1}{4}Q(\sin\tfrac{1}{2}\alpha)^{2S-2}(\cos\tfrac{1}{2}\alpha)^{2N-2S+2} , \quad (54)$$

$$A_{(kl)(mn)} = \tfrac{1}{8}Q(\sin\tfrac{1}{2}\alpha)^{2S-2}(\cos\tfrac{1}{2}\alpha)^{2N-2S}\cos\alpha ,$$
$$B_{(kl)(mn)} = -\tfrac{1}{8}Q(\sin\tfrac{1}{2}\alpha)^{2S-2}(\cos\tfrac{1}{2}\alpha)^{2N-2S} . \quad (55)$$

(b) *Regressive pairs* (SrN):

$$Z_{kl,mn} = -\tfrac{1}{4}Q(\sin\tfrac{1}{2}\alpha)^{2S-2}(\cos\tfrac{1}{2}\alpha)^{2N-2S+2} ,$$
$$Z_{lk,mn} = Z_{kl,mn} , \quad (56)$$

$$A_{(kl)(mn)} = -\tfrac{1}{4}Q(\sin\tfrac{1}{2}\alpha)^{2S-2}(\cos\tfrac{1}{2}\alpha)^{2N-2S+2} ,$$
$$B_{(kl)(mn)} = 0 . \quad (57)$$

(c) *Progressive pairs* (SpN):

Same expressions as for regressive pairs with opposite sign:

$$A_{(kl)(mn)} = \tfrac{1}{4}Q(\sin\tfrac{1}{2}\alpha)^{2S-2}(\cos\tfrac{1}{2}\alpha)^{2N-2S+2} ,$$
$$B_{(kl)(mn)} = 0 . \quad (58)$$

For illustration of Eqs. (54)–(58), amplitude and phase for the various transitions of a four-spin system are given in Fig. 8 as functions of the flip angle α of the mixing pulse. The phase ϕ is defined here as

$$\tan\phi = B_{(kl)(mn)}/A_{(kl)(mn)} ,$$

and describes the mixing between pure 2D absorption and 2D dispersion signals. The following conclusions about the general behavior of 2D spectra for weakly coupled spin $\frac{1}{2}$ systems can be drawn:

(1) The phase of peaks caused by regressive and progressive pairs is independent of the flip angle α. Regressive and progressive pairs have opposite sign;

(2) The phase of parallel pairs is dependent on the flip angle, changing by 90° for a variation of α from 0° to 180°. All parallel pairs have the same phase;

(3) For $\alpha = 0°$, only $1lN$ peaks have a nonvanishing intensity. Cross peaks are absent for $\alpha = 0°$;

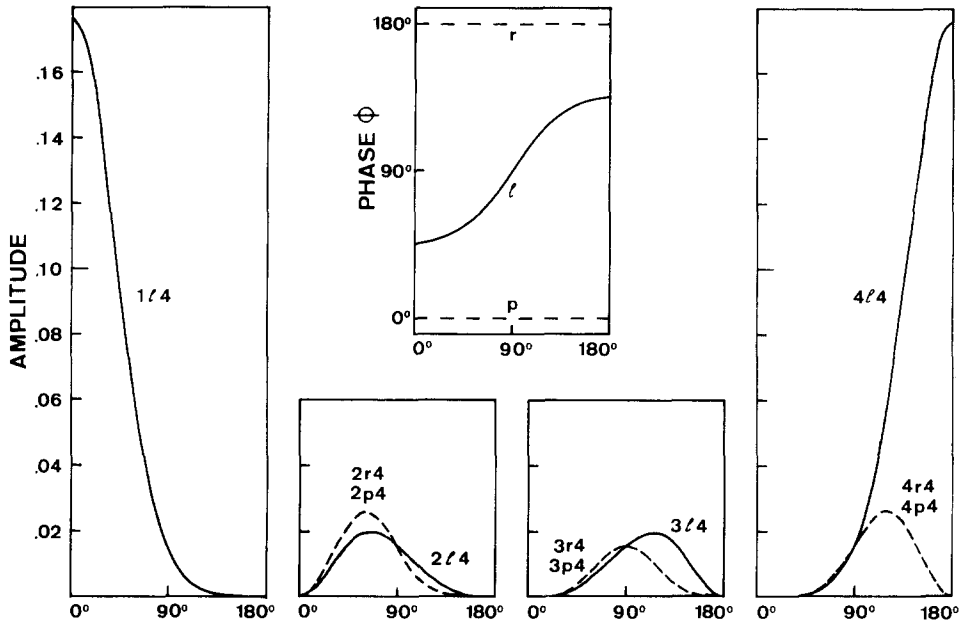

FIG. 8. Amplitude and phase for the various peaks in a 2D FTS of a system consisting of four nonequivalent nuclei as a function of the flip angle α of the mixing pulse.

(4) For a mixing pulse with $\alpha = 90°$, all cross peaks and dia peaks have the same absolute intensity. Parallel pairs cause peaks which are 90° out of phase in both ω_1 and ω_2 with respect to regressive and progressive pairs;

(5) For $\alpha = 180°$, only NlN peaks have a nonvanishing intensity. All spin polarizations will be inverted and only line pairs with completely reversed spin polarizations will produce cross-peaks in the 2D plot. These peaks are also responsible for the echo modulation in a conventional spin echo experiment.[29] The number of peaks in the 2D spectrum is equal to the number of peaks in a conventional 1D spectrum, namely $N \cdot 2^{N-1}$. Due to the small number of peaks in the 2D plot, the intensities are maximum in this case and are equal to the intensities of the dia peaks for $\alpha = 0°$;

(6) The optimum flip angle for maximum peak amplitude changes continuously from 0° to 180° for S increasing from 1 to N for parallel pairs. For regressive and progressive pairs, the same tendency is observed although the covered range of α_{opt} values is smaller;

(7) The attainable peak amplitude is minimum for pairs with $S \approx N/2$.

It is obvious that no cross peaks can occur for lines belonging to different molecules in a mixture. 2D FTS may, therefore, be used to single out the lines of the various molecules.

Experimental and theoretical 2D spectra for a weakly coupled two-spin system are shown in Figs. 9–12. The theoretical spectrum of Fig. 9 was computed based on the more general Eq. (61) for two 90° pulses. $S^{cc}(\omega_1, \omega_2)$ is shown. For true weak coupling, all 16 peaks would show the same absolute intensity, but the phases are unequal. All parallel pairs cause 2D dispersion peaks whereas regressive and progressive pairs generate cross peaks in 2D absorption with opposite signs for regressive and progressive pairs. Axial peaks have been neglected by setting $T_1 = \infty$.

A phase-sensitive 2D spectrum of a weakly coupled two-spin system is given in Fig. 10 with the same phase setting as in Fig. 9. The agreement is satisfactory taking into account the low resolution which is limited by the 64–64 data matrix used. Particularly, the 2D dispersion peaks are difficult to be represented with the present resolution, dictated by the restricted computer memory.

A much more satisfying representation can be obtained by plotting the absolute value spectrum, Eq. (7), as shown in Fig. 11. But clearly, the information content is lower.

The absolute value plot for a mixing pulse of 180° is given in Fig. 12. According to Eqs. (54)–(58), only four peaks (for parallel pairs) should occur. The four additional weak peaks seen are caused by deviations from the weak coupling character of the investigated spin system. From Figs. 10–12, it can be seen that axial peaks do occur, in general, for a 90° mixing pulse, but they are absent for a 180° mixing pulse.

It is possible to distinguish the three connectivity classes by performing one single experiment with a mixing pulse of 90°. To obtain more insight into the connectivity and to determine also the number of involved spins S, it is necessary to make measurements for several flip angles. Additionally, it is possible to enhance, selectively, certain peak amplitudes, by a suitable selection of the flip angle.

The conclusions drawn from the case of weak coupling can not be applied quantitatively to strongly coupled systems although the same tendencies can be observed for strong coupling, as will be shown in the next section. A direct generalization to systems with magnetically equivalent nuclei is not possible, either.

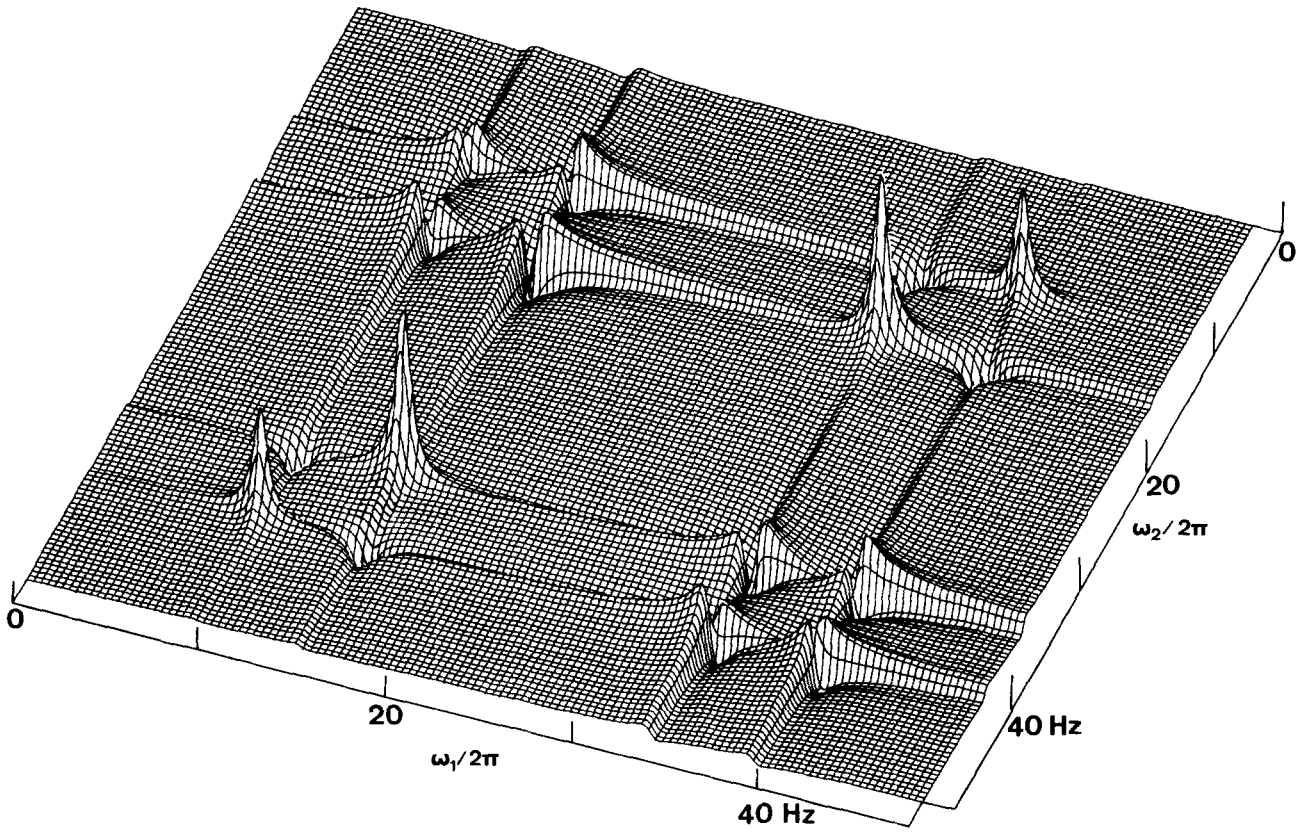

FIG. 9. Theoretical 2*D* FT spectrum of a two-spin system applying two 90° pulses to the system in equilibrium. The parameter values used correspond to the proton resonance of 2,3-dibromothiophene at 60 MHz. The weak coupling assumption was not used.

V. 2*D* FTS FOR A STRONGLY COUPLED TWO-SPIN SYSTEM

In this section, explicit results will be given for a strongly coupled two-spin system and compared with experimental results. It is assumed that the initial state $\sigma(0)$ is generated by means of a 90°_x pulse starting with a system in thermodynamic equilibrium. Then, the complex amplitude $Z_{kl,mn}$ is again given by Eq. (49).

The matrix representations of the two operators F_y and R in the eigenbase of the Hamiltonian are

$$F_y = \frac{i}{2} \cdot \begin{pmatrix} 0 & -u & -v & 0 \\ u & 0 & 0 & -u \\ v & 0 & 0 & -v \\ 0 & u & v & 0 \end{pmatrix}, \tag{59}$$

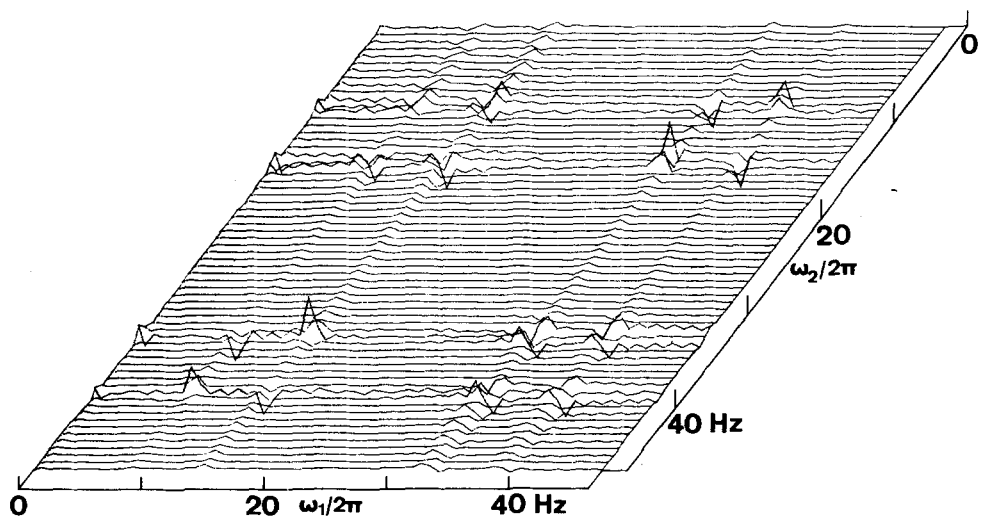

FIG. 10. Two-pulse experiment on 2,3-dibromothiophene. Flip angles for both pulses: 90°. 64 experiments with different pulse separation were used. A phase-sensitive spectrum is shown.

$$R=\begin{bmatrix} \cos^2(\tfrac{1}{2}\alpha) & -\tfrac{1}{2}iu\sin\alpha & -\tfrac{1}{2}iv\sin\alpha & -\sin^2(\tfrac{1}{2}\alpha) \\ -\tfrac{1}{2}iu\sin\alpha & \cos^2(\tfrac{1}{2}\alpha)-\sin2\theta\sin^2(\tfrac{1}{2}\alpha) & -\cos2\theta\sin^2(\tfrac{1}{2}\alpha) & -\tfrac{1}{2}iu\sin\alpha \\ -\tfrac{1}{2}iv\sin\alpha & -\cos2\theta\sin^2(\tfrac{1}{2}\alpha) & \cos^2(\tfrac{1}{2}\alpha)+\sin2\theta\sin^2(\tfrac{1}{2}\alpha) & -\tfrac{1}{2}iv\sin\alpha \\ -\sin^2(\tfrac{1}{2}\alpha) & -\tfrac{1}{2}iu\sin\alpha & -\tfrac{1}{2}iv\sin\alpha & \cos^2(\tfrac{1}{2}\alpha) \end{bmatrix}, \tag{60}$$

with $u=\cos\theta+\sin\theta$, $v=\cos\theta-\sin\theta$, and $\tan(2\theta)=2\pi J/(\Omega_1-\Omega_2)$. With Eqs. (27), (49), (59), and (60), one obtains finally the following real amplitudes for the strongly coupled two-spin system:

$$\begin{aligned}
&A_{(12)(12)}=\tfrac{1}{8}Q\cos^2(\tfrac{1}{2}\alpha)(1+\sin2\theta)(\cos\alpha-2\sin^2(\tfrac{1}{2}\alpha)\sin2\theta),\\
&B_{(12)(12)}=-\tfrac{1}{8}Q\cos^2(\tfrac{1}{2}\alpha)(1+\sin2\theta),\\
&A_{(12)(13)}=-\tfrac{1}{16}Q\sin^2\alpha\cos^2 2\theta,\\
&B_{(12)(13)}=0,\\
&A_{(12)(24)}=\tfrac{1}{8}Q\sin^2(\tfrac{1}{2}\alpha)(1+\sin2\theta)(2\cos^2(\tfrac{1}{2}\alpha)\\
&\qquad+\cos\alpha\cdot\sin2\theta),\\
&B_{(12)(24)}=-\tfrac{1}{8}Q\sin^2(\tfrac{1}{2}\alpha)(1+\sin2\theta)\sin2\theta,\\
&A_{(12)(34)}=\tfrac{1}{8}Q\sin^2(\tfrac{1}{2}\alpha)\cos\alpha\cos^2 2\theta,\\
&B_{(12)(34)}=-\tfrac{1}{8}Q\sin^2(\tfrac{1}{2}\alpha)\cos^2 2\theta,\\
&A_{(13)(13)}=\tfrac{1}{8}Q\cos^2(\tfrac{1}{2}\alpha)(1-\sin2\theta)(\cos\alpha+2\sin^2(\tfrac{1}{2}\alpha)\sin2\theta),\\
&B_{(13)(13)}=-\tfrac{1}{8}Q\cos^2(\tfrac{1}{2}\alpha)(1-\sin2\theta),\\
&A_{(13)(34)}=\tfrac{1}{8}Q\sin^2(\tfrac{1}{2}\alpha)(1-\sin2\theta)(2\cos^2(\tfrac{1}{2}\alpha)\\
&\qquad-\cos\alpha\cdot\sin2\theta),\\
&B_{(13)(34)}=\tfrac{1}{8}Q\sin^2(\tfrac{1}{2}\alpha)(1-\sin2\theta)\sin2\theta.
\end{aligned} \tag{61}$$

The remaining 10 cross and dia peaks of the two-spin system can be obtained from the C_{2v} symmetry of the corresponding $2D$ spectrum. For weak coupling, $\theta=0$, Eq. (61) reduces to Eqs. (55), (57), and (58).

Equation (61) demonstrates the following complications caused by the strong coupling (compare Sec. IV):

(1) The phase of the peaks caused by progressive pairs becomes dependent on the flip angle α, whereas the phase of the peaks caused by regressive pairs remains independent of α for arbitrary coupling strength;

(2) The phase change of the dia peaks for a variation of α from 0° to 180° is different from 90°. The corresponding phase change for cross peaks caused by parallel pairs is still 90°;

(3) For $\alpha=0°$, the dia peaks have all the same phase and the same relative intensities as in the slow passage spectrum;

(4) For a mixing pulse $\alpha=90°$ no equality of the absolute intensities is obtained, but the $2D$ absolute value spectrum has D_{4h} symmetry with the three intensity values

$$\begin{aligned}
&[A^2_{(13)(13)}+B^2_{(13)(13)}]^{1/2}=\tfrac{1}{16}Q(1-\sin2\theta)\sqrt{1+\sin^2 2\theta},\\
&[A^2_{(12)(12)}+B^2_{(12)(12)}]^{1/2}=\tfrac{1}{16}Q(1+\sin2\theta)\sqrt{1+\sin^2 2\theta},\\
&[A^2_{(12)(13)}+B^2_{(12)(13)}]^{1/2}=\tfrac{1}{16}Q\cos^2 2\theta;
\end{aligned} \tag{62}$$

(5) For $\alpha=180°$, a total of eight peaks occur: four $2l2$ peaks and four $2p2$ peaks. Only the dia peaks and the regressive peaks are suppressed. The following three absolute intensities occur:

$$\begin{aligned}
&[A^2_{(12)(34)}+D^2_{(12)(34)}]^{1/2}=\tfrac{1}{8}Q\sqrt{2}\cos^2 2\theta,\\
&[A^2_{(12)(24)}+D^2_{(12)(24)}]^{1/2}=\tfrac{1}{8}Q\sqrt{2}\sin2\theta(1+\sin2\theta),\\
&[A^2_{(13)(34)}+D^2_{(13)(34)}]^{1/2}=\tfrac{1}{8}Q\sqrt{2}\sin2\theta(1-\sin2\theta);
\end{aligned} \tag{63}$$

(6) The dependence of the optimum flip angle for maximum peak amplitude is similar to the case of weak coupling.

Experimental spectra for a strongly coupled two-spin system are shown in Figs. 13 and 14 for a mixing pulse

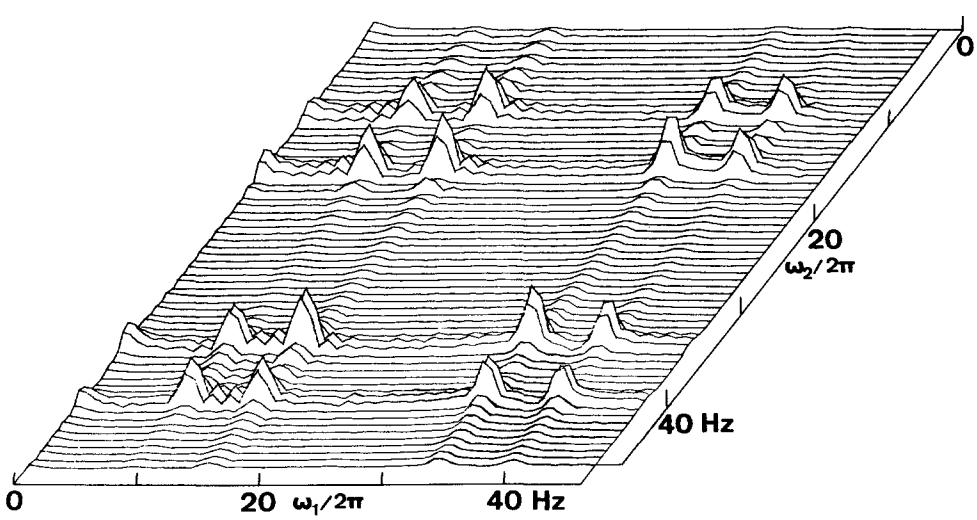

FIG. 11. Two pulse experiment on 2,3-dibromothiophene. Flip angles for both pulses: 90°. An absolute value spectrum is shown.

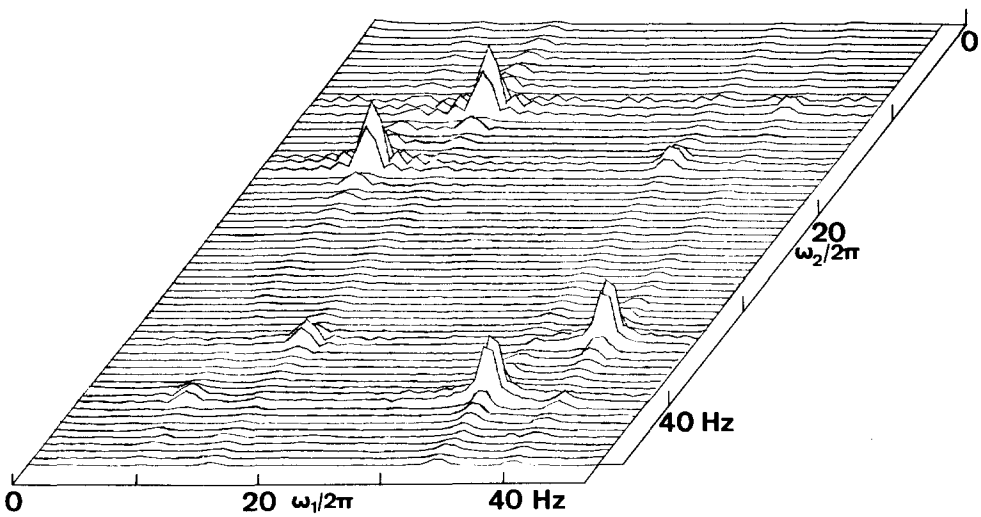

FIG. 12. Two-pulse experiment on 2,3-dibromothiophene with 180° mixing pulse. An absolute value spectrum is shown.

of 90° and 180°, respectively. They confirm the predictions based on Eq. (61).

VI. SYSTEMS WITH MAGNETICALLY EQUIVALENT SPINS

In close analogy to the calculation of 1*D* spectra, it is possible to introduce a group spin G for magnetically equivalent spins.[27] The 2*D* spectrum can then be divided into subspectra associated with definite quantum numbers for the various group spins. No cross peaks will occur between transitions belonging to different subspectra.

The AX_2 system may serve as an example. It is again assumed that the initial state $\sigma(0)$ is prepared by a 90°_x pulse acting on a system in thermodynamic equilibrium. Then, the complex amplitudes $Z_{kl,mn}$ are given by Eq. (49). F_y can be written as

$$F_y = (G_y^{(1)} \oplus G_y^{(0)}) + I_{Ay} . \tag{64}$$

Here, $G_y^{(p)}$ is the y-component spin angular momentum operator for a group spin p of the two X spins. For the rotation operator R, one obtains similarly

$$\begin{aligned} R = e^{-i\alpha F_x} &= (e^{-i\alpha G_x^{(1)}} \oplus e^{-i\alpha G_x^{(0)}}) e^{-i\alpha I_{Ax}} \\ &= \{[1^{(1)} - (1-\cos\alpha) G_x^{(1)2} - i \sin\alpha G_x^{(1)}] \oplus 1^{(0)}\} \\ &\quad \times [\cos\tfrac{1}{2}\alpha 1^{(1/2)} - 2i \sin\tfrac{1}{2}\alpha I_{Ax}] . \end{aligned} \tag{65}$$

The eigenfunctions of the AX_2 system are numbered in the following manner: $\phi_1 = \alpha\alpha\alpha$, $\phi_2 = \beta\alpha\alpha$, $\phi_3 = (\alpha\alpha\beta + \alpha\beta\alpha)/\sqrt{2}$, $\phi_4 = (\beta\alpha\beta + \beta\beta\alpha)/\sqrt{2}$, $\phi_5 = \alpha\beta\beta$, $\phi_6 = \beta\beta\beta$, $\phi_7 = (\alpha\alpha\beta - \alpha\beta\alpha)/\sqrt{2}$ and $\phi_8 = (\beta\alpha\beta - \beta\beta\alpha)/\sqrt{2}$. The energy level diagram is indicated in Fig. 15. Three pairs of transitions are degenerate.

Based on Eqs. (27), (49), (64), and (65) one finds the following real amplitudes for the 2*D* spectrum:

$$A_{(12)(12)} = A_{(56)(56)} = \tfrac{1}{8} Q \cos^4(\tfrac{1}{2}\alpha) \cos\alpha ,$$

$$B_{(12)(12)} = B_{(56)(56)} = -\tfrac{1}{8} Q \cos^4(\tfrac{1}{2}\alpha) ,$$

$$A_{(34)(34)} = \tfrac{1}{8} Q \cos^3\alpha ; \quad B_{(34)(34)} = -\tfrac{1}{8} Q \cos^2\alpha ,$$

$$A_{(78)(78)} = \tfrac{1}{8} Q \cos\alpha ; \quad B_{(78)(78)} = -\tfrac{1}{8} Q ,$$

$$A_{(12)(34)} = A_{(56)(34)} = \tfrac{1}{16} Q \sin^2\alpha\cos\alpha ,$$

$$B_{(12)(34)} = B_{(56)(35)} = -\tfrac{1}{16} Q \sin^2\alpha ,$$

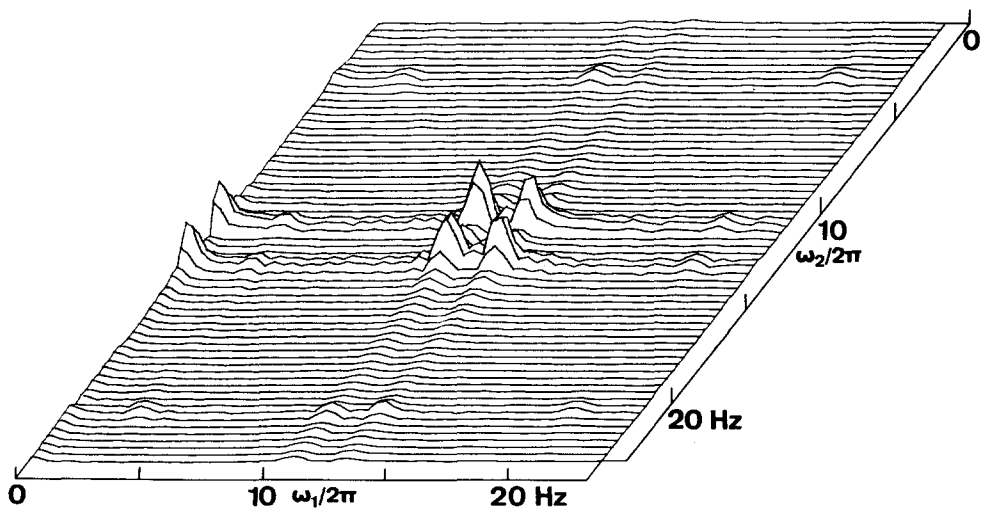

FIG. 13. Two-pulse experiment on 2,3,4-trichloronitrobenzene with a 90° mixing pulse. An absolute value spectrum is shown.

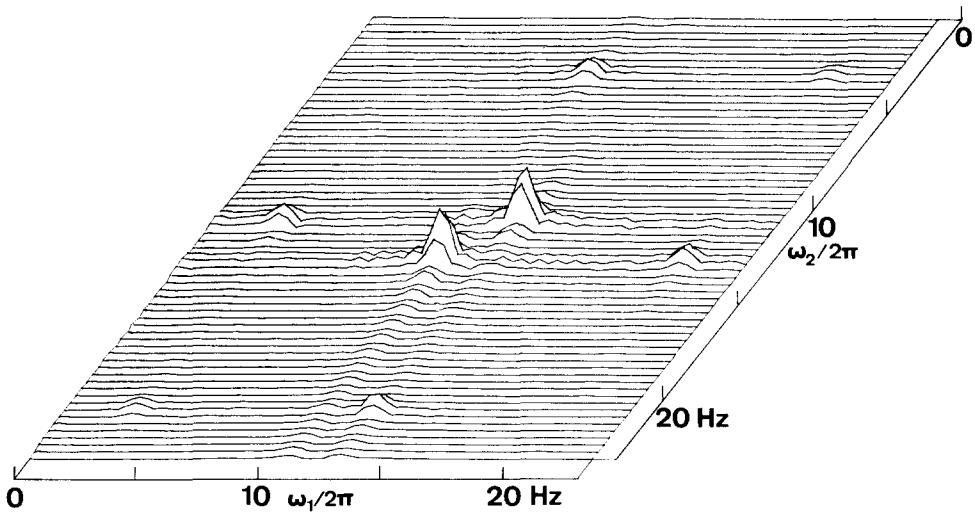

FIG. 14. Two-pulse experiment on 2,3,4-trichloronitrobenzene with a 180° mixing pulse. An absolute value spectrum is shown.

$$A_{(12)(56)} = \tfrac{1}{8} Q \sin^4(\tfrac{1}{2}\alpha)\cos\alpha; \quad B_{(12)(56)} = -\tfrac{1}{8} Q \sin^4(\tfrac{1}{2}\alpha),$$

$$A_{\binom{13}{35}\binom{13}{35}} = A_{\binom{24}{46}\binom{24}{46}} = \tfrac{1}{2} Q \cos^2(\tfrac{1}{2}\alpha)\cos\alpha ,$$

$$B_{\binom{13}{35}\binom{13}{35}} = B_{\binom{24}{46}\binom{24}{46}} = -\tfrac{1}{2} Q \cos^2(\tfrac{1}{2}\alpha) ,$$

$$A_{\binom{13}{35}\binom{24}{46}} = \tfrac{1}{2} Q \sin^2(\tfrac{1}{2}\alpha)\cos\alpha ,$$

$$B_{\binom{13}{35}\binom{24}{46}} = -\tfrac{1}{2} Q \sin^2(\tfrac{1}{2}\alpha) , \qquad (66)$$

$$A_{(12)\binom{13}{35}} = A_{(56)\binom{24}{46}} = -A_{(12)\binom{24}{46}} = -A_{(56)\binom{13}{35}} = -\tfrac{1}{8} Q \sin^2\alpha,$$

$$B_{(12)\binom{13}{35}} = B_{(56)\binom{24}{46}} = -B_{(12)\binom{24}{46}} = -B_{(56)\binom{13}{35}} = 0 ,$$

$$A_{(34)\binom{13}{35}} = A_{(34)\binom{24}{46}} = B_{(34)\binom{13}{35}} = B_{(34)\binom{24}{46}} = 0 .$$

The amplitudes with multiple indices refer to degenerate transitions. A partial, experimental spectrum of the triplet region is shown in Fig. 15 for a mixing pulse of 90°. The experimental intensities agree well with the theoretical values for the relative intensities

$$\begin{bmatrix} 1 & 2 & 1 \\ 2 & 4 & 2 \\ 1 & 2 & 1 \end{bmatrix} .$$

All nine lines have the same phase.

The following conclusions can be drawn from this example: (1) the relative intensities of the dia peaks (1, 4, 1, 8, 8) for 90° flip angle are not equal to the intensities of the 1*D* spectrum (2, 4, 2, 8, 8). This is in contrast to the strongly coupled two-spin system; (2) for 90° flip angle, the central peak of the triplet is exclusively caused by the antisymmetric transition (78); (3) the cross peaks which relate transition (34) with the transitions $\binom{13}{35}$ and $\binom{24}{46}$ are zero for all flip angles. The reason for the disappearance of these cross peaks is that the transitions $\binom{13}{35}$ and $\binom{24}{46}$ are degenerate. They each contain a transition in regressive and a transition in progressive connection with transition (34). The regressive and progressive contributions are of opposite sign and cancel; (4) the phase relationships are similar to those for nonequivalent, weakly coupled spins. One can again easily distinguish parallel, regressive, and progressive pairs.

VII. 2*D* FTS IN THE PRESENCE OF AN INHOMOGENEOUS STATIC FIELD

In an inhomogenous static field, the various single quantum transition frequencies will become functions

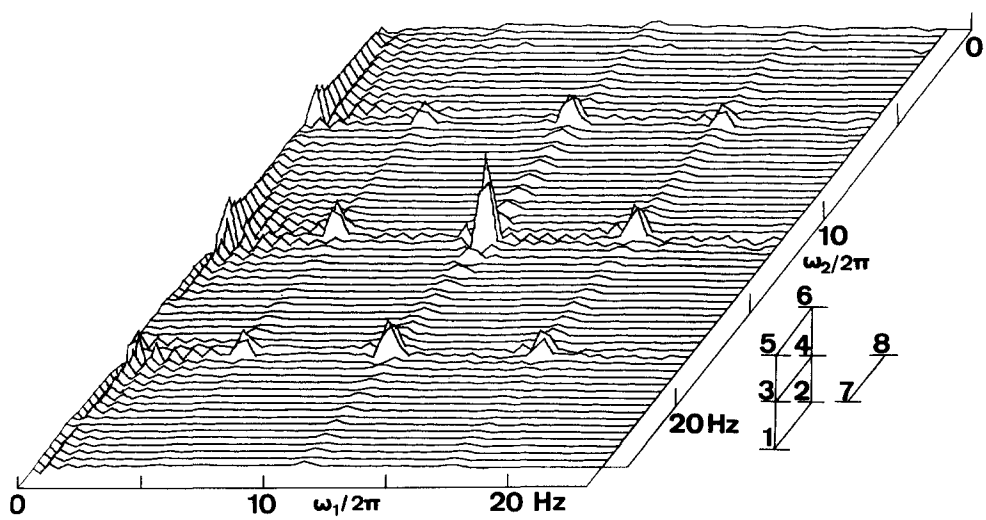

FIG. 15. Two-pulse experiment on 1,1,2-trichloroethane with a mixing pulse of 90°. A phase-sensitive plot is shown with the peaks caused by parallel pairs in absorption. A 2*D* filtering procedure has been employed to single out the region of the $CHCl_2$ triplet. The numbering of the energy levels for the AX_2 system is indicated.

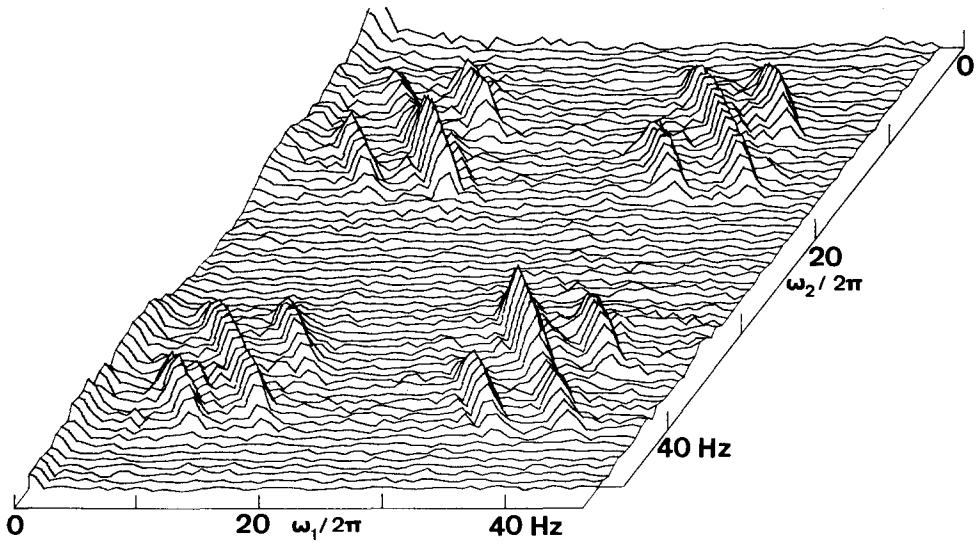

FIG. 16. Two-pulse experiment on 2,3-dibromothiophene with a 90° mixing pulse in a simulated inhomoeneous magnetic field. An absolute value plot is shown which should be compared with the corresponding 2*D* spectrum of Fig. 11, taken in a homogenous field.

of the spatial variable **r**:

$$\omega_{ik}(\mathbf{r}) = \omega_{ik} - \gamma \Delta H(\mathbf{r}) \ , \tag{67}$$

where $\Delta H(\mathbf{r})$ is the deviation of the local field from an arbitrary reference field. Accordingly, one obtains for the local signal contributions to the 2*D* spectrum

$$S(\mathbf{r}, \omega_1, \omega_2) = S(\omega_1 + \gamma \Delta H(\mathbf{r}), \omega_2 + \gamma \Delta H(\mathbf{r})) \ , \tag{68}$$

and for the signal integrated over the sample volume

$$\bar{S}(\omega_1, \omega_2) = \int\int\int d\tau c(\mathbf{r}) S(\omega_1 + \gamma \Delta H(\mathbf{r}), \omega_2 + \gamma \Delta H(\mathbf{r})) \ , \tag{69}$$

with the local spin density $c(\mathbf{r})$. It is evident that $\bar{S}(\omega_1, \omega_2)$ represents the original 2*D* spectrum $S(\omega_1, \omega_2)$ smeared along the main diagonal only, reducing the resolution along this diagonal. On the other hand, the resolution perpendicular to the main diagonal remains unaffected. This means that much of the inherent information can be retrieved even in an arbitrarily inhomogenous magnetic field. An example is given in Fig. 16. By cutting 1*D* cross sections through such a 2*D* spectrum, it is possible to obtain high resolution spectra in inhomogeneous magnetic fields. Clearly, these spectra are not equivalent to the conventional 1*D* spectra nor do they contain all the information of 1*D* spectra, but, in many cases, they contain enough information to solve a particular problem.

The information which can be retrieved even in the worst case is restricted to the distance of cross peaks from the main diagonal, i.e., it is possible to obtain coupling constants and relative chemical shifts of coupled nuclei. Uncoupled nuclei do not provide cross peaks and, consequently, their shifts can not be determined with more accuracy than in conventional spectroscopy. The retained resolution relies on the formation of difference frequencies within a molecular spin system which are completely independent of macroscopic field inhomogeneities.

It must be emphasized that the stringent requirement for magnetic field stability remains. The field-frequency stability must stay within the resolution limit to be achieved over the entire experiment time. A combination with difference frequency spectroscopy[28] to loosen this requirement is at least not obvious. This means that experiments in inhomogeneous fields require a particularly stable field-frequency lock or a superconducting magnet with an inherently sufficient long-term stability.

A 2*D* FTS experiment in an inhomogeneous static magnetic field resembles a spin echo experiment. The echo envelope is modulated by the various spin–spin coupling constants,[29] and it is the source for the so-called *J* spectra.[30] They permit the determination of spin–spin coupling constants with high accuracy. The information content of 2*D* spectra is considerably higher as chemical shifts can be determined as well.

VIII. OBSERVATION OF ZERO AND DOUBLE QUANTUM TRANSITIONS

2*D* FTS offers a unique possibility to observe zero quantum ($\Delta M = 0$),[31] double quantum ($\Delta M = \pm 2$), and multiple quantum transitions. It is known that double quantum transitions can be observed in slow passage experiments when sufficiently strong rf fields are applied.[32] They do not appear in single pulse Fourier experiments.[3] Zero quantum transitions can neither be observed with slow passage nor with conventional Fourier experiments.

The condition for the occurrence of $\Delta M = 0$ or $|\Delta M| \geq 2$ peaks in a 2*D* spectrum is that the density operator $\sigma(0)$ at the beginning of the evolution period contains matrix elements connecting eigenvalues with $\Delta M = 0$ or $|\Delta M| \geq 2$. These elements oscillate during the evolution period with zero quantum, double quantum, or with higher transition frequencies. Elements of this kind do not directly produce observable transverse magnetization, but it is possible to transform them into transverse magnetization components by means of the mixing pulse at $t = t_1$. By performing a sequence of experiments with various t_1 values, it is possible to trace

out the time evolution of these unobservable matrix elements.

The complex signal amplitudes $Z_{kl,mn}$ of the resulting $2D$ spectrum can again be computed by means of Eq. (27). Under the assumption of weak coupling among N nonequivalent spins $\frac{1}{2}$, one obtains in analogy to Eq. (51) the expression

$$Z_{kl,mn} = \frac{i}{2} N\gamma\hbar(-1)^{\Delta_{lm}}(i)^{\Delta_{lm}+\Delta_{kn}}[\sin\tfrac{1}{2}\alpha]^{\Delta_{lm}+\Delta_{kn}} \times[\cos\tfrac{1}{2}\alpha]^{2N-\Delta_{lm}-\Delta_{kn}}\sigma(0)_{mn}(M_l - M_k) \,. \tag{70}$$

A few possibilities to prepare a state $\sigma(0)$ with $\Delta M = 0$ or $|\Delta M| \geq 2$ elements are: (1) selective 180° pulse on a single transition followed immediately by a nonselective 90° pulse; (2) selective saturation of one transition followed by a nonselective 90° pulse; and (3) nonselective 90° pulse followed after a suitable delay τ by a second nonselective 90° pulse.

To see the implications of Eq. (70) more clearly, the weakly coupled two-spin system will be investigated in more detail. It is assumed that the system has been prepared in a nonequilibrium state of first kind[20] with the populations P_1, P_2, P_3, and P_4. A 90°_x pulse at time $t = 0$ generates then the following initial density operator $\sigma(0)$:

$$\sigma(0) = R_x(\pi/2)\cdot\begin{pmatrix} P_1 & 0 & 0 & 0 \\ 0 & P_2 & 0 & 0 \\ 0 & 0 & P_3 & 0 \\ 0 & 0 & 0 & P_4 \end{pmatrix}\cdot R_x^{-1}(\pi/2)$$

$$= \frac{1}{4}\begin{pmatrix} (P_1+P_2+P_3+P_4) & i(P_1-P_2+P_3-P_4) & i(P_1+P_2-P_3-P_4) & (-P_1+P_2+P_3-P_4) \\ i(-P_1+P_2-P_3+P_4) & (P_1+P_2+P_3+P_4) & (P_1-P_2-P_3+P_4) & i(P_1+P_2-P_3-P_4) \\ i(-P_1-P_2+P_3+P_4) & (P_1-P_2-P_3+P_4) & (P_1+P_2+P_3+P_4) & i(P_1-P_2+P_3-P_4) \\ (-P_1+P_2+P_3-P_4) & i(-P_1-P_2+P_3+P_4) & i(-P_1+P_2-P_3+P_4) & (P_1+P_2+P_3+P_4) \end{pmatrix} . \tag{71}$$

Here, the $\Delta M = 0$, off-diagonal elements are $\sigma(0)_{23}$ and $\sigma(0)_{32}$, the $\Delta M = 2$ element is $\sigma(0)_{14}$ and the $\Delta M = -2$ element is $\sigma(0)_{41}$. It is seen that these elements are different from zero whenever $P_1 + P_4 \neq P_2 + P_3$.

To compute the time evolution during the evolution period, it is best to consider the system in a frame rotating with the carrier frequency ω of the applied rf pulses which is also used to demodulate the received rf signal. Because $\sigma^r(0) = \sigma(0)$, one obtains

$$\sigma^r(t_1)_{kl} = \sigma(0)_{kl} \times \exp\{-i(\mathcal{H}_{kk} - \omega F_{z\,kk})t_1 + i(\mathcal{H}_{ll} - \omega F_{z\,ll})t_1 - t_1/T_{2kl}\} . \tag{72}$$

For the oscillation frequencies of zero and double quantum transitions, one finds:

zero quantum transition: $$\Delta\omega_0 = \mathcal{H}_{22} - \mathcal{H}_{33} = \Omega_1 - \Omega_2 \,, \tag{73}$$

double quantum transition: $$\Delta\omega_2 = \mathcal{H}_{11} - \mathcal{H}_{44} - 2\omega = \Omega_1 + \Omega_2 - 2\omega \,, \tag{74}$$

where Ω_1 and Ω_2 are the Larmor frequencies of the two nuclei. The frequency of the double quantum transition is independent of the spin–spin coupling constant J, even for strong coupling. The frequency of the zero quantum transition, on the other hand, is, for strong coupling, given by

$$\Delta\omega_0 = \sqrt{(\Omega_1 - \Omega_2)^2 + (2\pi J)^2} \,. \tag{75}$$

With an rf pulse with flip angle α at time $t = t_1$, one obtains the observable magnetization which is used to compute a $2D$ spectrum with the following complex and real amplitudes:

Zero quantum transition:

$$Z_{12,23} = \tfrac{1}{2}N\gamma\hbar\sin\tfrac{1}{2}\alpha[\cos\tfrac{1}{2}\alpha]^3\sigma(0)_{23} \,,$$
$$Z_{21,23} = -\tfrac{1}{2}N\gamma\hbar[\sin\tfrac{1}{2}\alpha]^3[\cos\tfrac{1}{2}\alpha]\sigma(0)_{23} \,, \tag{76}$$

and

$$A_{(12)(23)} = \tfrac{1}{8}N\gamma\hbar\sin\alpha\cos\alpha\,\mathrm{Re}\{\sigma(0)_{23}\} \,,$$
$$B_{(12)(23)} = \tfrac{1}{8}N\gamma\hbar\sin\alpha\,\mathrm{Re}\{\sigma(0)_{23}\} \,,$$
$$C_{(12)(23)} = \tfrac{1}{8}N\gamma\hbar\sin\alpha\cos\alpha\,\mathrm{Im}\{\sigma(0)_{23}\} \,, \tag{77}$$
$$D_{(12)(23)} = \tfrac{1}{8}N\gamma\hbar\sin\alpha\,\mathrm{Im}\{\sigma(0)_{23}\} \,,$$

with the relations

$$A_{(13)(23)} = -A_{(24)(23)} = -A_{(34)(23)} = A_{(12)(23)} \,,$$
$$-B_{(13)(23)} = B_{(24)(23)} = -B_{(34)(23)} = B_{(12)(23)} \,,$$
$$C_{(13)(23)} = -C_{(24)(23)} = -C_{(34)(23)} = C_{(12)(23)} \,, \tag{78}$$
$$-D_{(13)(23)} = D_{(24)(23)} = -D_{(34)(23)} = D_{(12)(23)} \,.$$

Double quantum transition:

$$Z_{12,14} = \tfrac{1}{2}N\gamma\hbar[\sin\tfrac{1}{2}\alpha]^3[\cos\tfrac{1}{2}\alpha]\sigma(0)_{14} \,,$$
$$Z_{21,14} = -\tfrac{1}{2}N\gamma\hbar\sin\tfrac{1}{2}\alpha[\cos\tfrac{1}{2}\alpha]^3\sigma(0)_{14} \,, \tag{79}$$

and

$$A_{(12)(14)} = -\tfrac{1}{8}N\gamma\hbar\sin\alpha\cos\alpha\,\mathrm{Re}\{\sigma(0)_{14}\} \,,$$
$$B_{(12)(24)} = \tfrac{1}{8}N\gamma\hbar\sin\alpha\,\mathrm{Re}\{\sigma(0)_{14}\} \,,$$

$$C_{(12)(14)} = -\tfrac{1}{8}N\gamma\hbar \sin\alpha\cos\alpha \,\mathrm{Im}\{\sigma(0)_{14}\}\ ,$$

$$D_{(12)(24)} = \tfrac{1}{8}N\gamma\hbar \sin\alpha \,\mathrm{Im}\{\sigma(0)_{14}\}\ , \qquad (80)$$

with the relations

$$A_{(13)(14)} = -A_{(24)(14)} = -A_{(34)(14)} = A_{(12)(14)}\ ,$$

$$B_{(13)(14)} = -B_{(24)(14)} = -B_{(34)(14)} = B_{(12)(14)}\ ,$$

$$C_{(13)(14)} = -C_{(24)(14)} = -C_{(34)(14)} = C_{(12)(14)}\ ,$$

$$D_{(13)(14)} = -D_{(24)(14)} = -D_{(34)(14)} = D_{(12)(14)}\ .$$

It is interesting to note that the oscillation frequency of the zero quantum transition, Eq. (75), is, to a large extent, independent of the magnetic field strength and magnetic field homogeneity and completely independent of the carrier frequency ω. The ω_1 coordinate of the zero quantum peaks in a 2*D* spectrum is therefore dependent only on the inherent properties of the spin system and not on performance conditions.

The oscillation frequency of the double quantum transition, Eq. (74), on the other hand, changes with 2ω when the carrier frequency is moved. Unlike double quantum transitions in slow passage spectra, the double quantum transition in 2*D* spectroscopy does not occur in the center of the two doublets, but its position is strongly dependent on the carrier frequency ω.

An experimental spectrum is shown in Fig. 17. It is the result of a three pulse experiment. The first two 90° pulses with a separation of 236 ms were employed to create an initial density operator $\sigma(0)$ with $\Delta M = 0$ and $\Delta M = \pm 2$ matrix elements. The third pulse at $t = t_1$ was a mixing pulse with $\alpha = 90°$. Zero and double quantum peaks have about the same intensities as the single quantum peaks, in this particular case. The relative intensities strongly depend on the separation of the first two pulses.

IX. EXPERIMENTAL

The experimental results presented in this paper have been obtained by means of a Varian DA60 high resolution NMR spectrometer equipped with an internal fluorine field-frequency lock and with pulse equipment to perform Fourier experiments. The data processing was done on a Varian 620i computer which was interfaced to the spectrometer and which contained 16*k* core memory and was equipped with the usual peripherals.

Due to the limited core memory, the data matrix had to be restricted to 64×64 accumulated samples from 64 experiments for different pulse spacings t_1. For the data processing, a slightly modified computer program, used earlier for Fourier zeugmatography,[19] was utilized. For each complex 1*D* Fourier transformation, the array of 64 samples was augmented by 64 zeros[33] such that, finally, each of the four real components S^{cc}, S^{ss}, S^{cs}, and S^{sc} was again represented by 64×64 sample values.

The phase of the 2*D* spectrum was adjusted by a suitable linear combination of S^{cc}, S^{ss}, S^{cs}, and S^{sc}. No frequency-dependent phase shift was employed.

2*D* spectra were plotted either by means of a teletype, using a letter code to indicate signal amplitudes, or by means of an *xy*-plotter plotting parallel cross sections to give the impression of a 3*D* representation.

It is clear that the shown experimental results are preliminary in many respects. The main limitation of the present setup is the restricted number of samples which can be stored in computer memory.

There are several possibilities to solve this problem:

(1) *Partial spectra*: By means of suitable 2*D* filtering procedures, it is possible to obtain partial 2*D* spectra. An example is shown in Fig. 15.

(2) *Calculation of cross sections*: In many cases, it is sufficient to represent the 2*D* spectra by a set of parallel cross sections, e.g., through the major signal peaks. A simple possibility is to select after the first Fourier transformation those samples which lie in the center of a resonance line and to reject all other samples to reduce the storage and computational requirements.

(3) *Use of bulk storage*: The use of a disc memory may permit one to record and process up to 1000

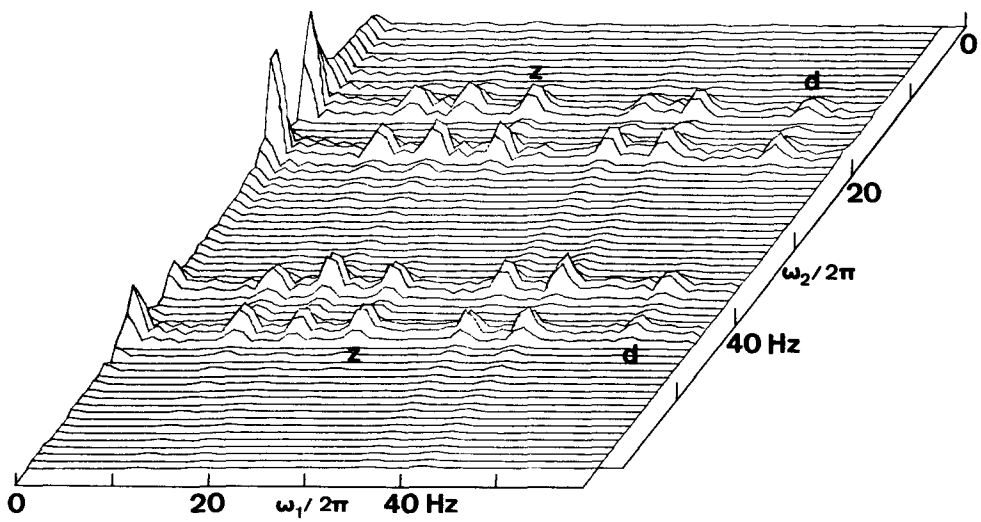

FIG. 17. Three-pulse experiment on 2,3-dibromothiophene using three 90° pulses. The separation of the first and the second rf pulses was 236 ms. The 2*D* spectrum shows the zero (z) and double quantum transitions (d) of the weakly coupled two-spin system.

$\times 1000$ data matrices.

A second limitation is the present facilities for the representation of $2D$ spectra. A considerable improvement of the visual impression is possible either with a matrix plotter or by means of a CRT display.

X. CONCLUSIONS

In this paper, the two-pulse version of $2D$ spectroscopy has been treated in explicit detail. The general formalism has been formulated to permit the description of a much larger class of experiments. Many extensions have briefly been mentioned in Sec. II. They will be described in more detail in further papers. The experimental aspects of $2D$ data processing will also be treated at another place.

The described experiments and the explicit calculations have been restricted to particularly simple cases, to systems with weakly coupled nuclei and to the strongly coupled two-spin system. For the case of three or more strongly coupled spins, it is convenient to take recourse to a numerical simulation of $2D$ spectra by means of a digital computer.[16]

$2D$ spectroscopy fascinates by its conceptual simplicity and by its general applicability. It seems to open one further dimension to the spectroscopist. Of particular interest are the possibilities to determine the relations between the various transitions of a spectrum, to measure double quantum transitions, to obtain high-resolution spectra in inhomogeneous magnetic fields, and to image macroscopic objects by measuring the $2D$ or $3D$ spin density. Intriguing applications are also possible in carbon-13 resonance in liquids and in solids by measuring $2D$-resolved carbon-13 spectra.

The basic principles which have been exploited are very general and can be applied to other coherent spectroscopies as well. Applications are conceivable in electron spin resonance, nuclear quadrupole resonance, in microwave rotational spectroscopy, and possibly in laser infrared spectroscopy.

ACKNOWLEDGMENTS

This research was supported in parts by the Swiss National Science Foundation. Several illuminating discussions with Professor J. Jeener are acknowledged. The authors are grateful to Dr. Anil Kumar, Mr. Luciano Müller, Mr. Stefan Schäublin, and Mr. Dieter Welti for many comments and Mr Alexander Wokaun for a careful, critical reading of the manuscript. Technical and computational support was provided by Mr. Kurt Brunner, Mr. Alexander Frey, Mr. Hansrudolf Hager, and Mr. Jürg Keller.

[1] S. Goldman, *Information Theory* (Dover, New York, 1968); B. M. Brown, *The Mathematical Theory of Linear Systems* (Science, New York, 1965).
[2] P. B. Fellgett (Thesis, University of Cambridge, 1951); G. A. Vanasse and H. Sakai, Prog. Opt. **6**, 259 (1967); R. J. Bell, *Introductory Fourier Transform Spectroscopy* (Academic, New York, 1972).
[3] R. R. Ernst and W. A. Anderson, Rev. Sci. Instrum. **37**, 93 (1966); R. R. Ernst, Adv. in Magn. Reson. **2**, 1 (1966); T. C. Farrar and E. D. Becker, *Pulse and Fourier Transform* NMR (Academic, New York, 1971).
[4] D. Ziessow, *On-line Rechner in der Chemie* (de Gruyter, Berlin, 1973).
[5] A. Abragam, *The Principles of Nuclear Magnetism* (Oxford, University, New York, 1961), Chap. XII.
[6] R. K. Harris and K. M. Worvill, J. Magn. Reson. **9**, 394 (1973); R. K. Harris, N. C. Pyper, and K. M. Worvill, J. Magn. Reson. **18**, 139 (1975).
[7] F. Bloch, Phys. Rev. **111**, 841 (1958).
[8] W. A. Anderson and R. Freeman, J. Chem. Phys. **37**, 85 (1962).
[9] R. Freeman and W. A. Anderson, J. Chem. Phys. **37**, 2053 (1962).
[10] E. B. Baker, J. Chem. Phys. **37**, 911 (1962).
[11] S. Sørensen, R. S. Hansen and H. J. Jakobsen, J. Magn. Reson. **14**, 243 (1974).
[12] E. L. Hahn, Phys. Rev. **80**, 580 (1950).
[13] R. L. Vold, J. S. Waugh, M. P. Klein, and D. E. Phelps, J. Chem. Phys. **48**, 3831 (1968); R. Freeman and H. D. W. Hill, J. Chem. Phys. **54**, 3367 (1971).
[14] R. Freeman, J. Chem. Phys. **53**, 457 (1970).
[15] F. Günther, Ann. Phys. **7**, 396 (1971).
[16] J. Jeener and G. Alewaeters (private communication).
[17] R. R. Ernst, Chimia **29**, 179 (1975).
[18] R. R. Ernst, J. Magn. Reson. **3**, 10 (1970); E. Bartholdi, A. Wokaun, and R. R. Ernst (to be published).
[19] A. Kumar, D. Welti, and R. R. Ernst, J. Magn. Reson. **18**, 69 (1975).
[20] S. Schäublin, A. Höhener, and R. R. Ernst, J. Magn. Reson. **13**, 196 (1974); S. Schäublin, A. Wokaun, and R. R. Ernst (to be published).
[21] L. Müller, A. Kumar, and R. R. Ernst, J. Chem. Phys. **63**, 5490 (1975).
[22] A. Pines, M. G. Gibby, and J. S. Waugh, J. Chem. Phys. **59**, 569 (1973).
[23] L. Müller, A. Kumar, T. Baumann, and R. R. Ernst, Phys. Rev. Lett. **32**, 1402 (1974); R. K. Hester, J. L. Ackerman, V. R. Gross, and J. S. Waugh, Phys. Rev. Lett. **34**, 993 (1975).
[24] J. S. Waugh (private communication).
[25] Superoperators (also called Liouville operators), are indicated by $\hat{}$; see C. N. Banwell and H. Primas, Mol. Phys. **6**, 225 (1963).
[26] A. G. Redfield, Adv. Magn. Reson. **1**, 1 (1965).
[27] P. L. Corio, *Structures of High-Resolution* NMR *Spectra* (Academic, New York, 1966).
[28] R. R. Ernst, J. Magn. Reson. **4**, 280 (1971).
[29] E. L. Hahn and D. E. Maxwell, Phys. Rev. **88**, 1070 (1952).
[30] R. Freeman and H. D. W. Hill, J. Chem. Phys. **54**, 301 (1971).
[31] The notion "zero quantum transition" is not strictly correct. These transitions are also double quantum transition, one quantum being absorbed and one being emitted.
[32] S. Yatsiv, Phys. Rev. **113**, 1522 (1959).
[33] E. Bartholdi and R. R. Ernst, J. Magn. Reson. **11**, 9 (1973).